Article

Current Biology

Ordovician origin and subsequent diversification of the brown algae

Highlights

- Brown algal phylogeny and evolutionary timeline were established with plastid genomes
- Brown algae originated during the late Ordovician Period (ca. 450 Ma)
- The major diversification of brown algae occurred during the Mesozoic Era
- Isogamy reappearances correlate with gametic parthenogenesis

Authors

Seok-Wan Choi, Louis Graf, Ji Won Choi, ..., Andrew H. Knoll, Robert A. Andersen, Hwan Su Yoon

Correspondence

hsyoon2011@skku.edu

In brief

Brown algae exhibit complex multicellularity and diverse gamete types; however, the timing and mechanisms of the evolution remain unclear. Choi et al. show that brown algae emerged with diversification of marine invertebrates during the Ordovician Period. Further diversification and transitions in gamete types occurred during the Mesozoic Era.

Choi et al., 2024, Current Biology *34*, 1–15
February 26, 2024
https://doi.org/10.1016/j.cub.2023.12.069

CellPress

Current Biology

CellPress

Article

Ordovician origin and subsequent diversification of the brown algae

Seok-Wan Choi,[1] Louis Graf,[1,2] Ji Won Choi,[1] Jihoon Jo,[1,3] Ga Hun Boo,[1] Hiroshi Kawai,[4] Chang Geun Choi,[5] Shuhai Xiao,[6] Andrew H. Knoll,[7] Robert A. Andersen,[8] and Hwan Su Yoon[1,9,*]

[1]Department of Biological Sciences, Sungkyunkwan University, Suwon 16419, Republic of Korea
[2]Institut de Biologie de l'École Normale Supérieure, Université Paris Sciences et Lettres, Paris 75005, France
[3]Honam National Institute of Biological Resources, Mokpo 58762, Republic of Korea
[4]Kobe University Research Center for Inland Seas, Rokkodai, Nadaku, Kobe 657-8501, Japan
[5]Department of Ecological Engineering, College of Environmental and Marine Technology, Pukyong National University, Busan 48513, Republic of Korea
[6]Department of Geosciences, Virginia Tech, Blacksburg, VA 24061, USA
[7]Department of Organismic and Evolutionary Biology, Harvard University, Cambridge, MA 02138, USA
[8]Friday Harbor Laboratories, University of Washington, Seattle, WA 98250, USA
[9]Lead contact
*Correspondence: hsyoon2011@skku.edu
https://doi.org/10.1016/j.cub.2023.12.069

SUMMARY

Brown algae are the only group of heterokont protists exhibiting complex multicellularity. Since their origin, brown algae have adapted to various marine habitats, evolving diverse thallus morphologies and gamete types. However, the evolutionary processes behind these transitions remain unclear due to a lack of a robust phylogenetic framework and problems with time estimation. To address these issues, we employed plastid genome data from 138 species, including heterokont algae, red algae, and other red-derived algae. Based on a robust phylogeny and new interpretations of algal fossils, we estimated the geological times for brown algal origin and diversification. The results reveal that brown algae first evolved true multicellularity, with plasmodesmata and reproductive cell differentiation, during the late Ordovician Period (ca. 450 Ma), coinciding with a major diversification of marine fauna (the Great Ordovician Biodiversification Event) and a proliferation of multicellular green algae. Despite its early Paleozoic origin, the diversification of major orders within this brown algal clade accelerated only during the Mesozoic Era, coincident with both Pangea rifting and the diversification of other heterokont algae (e.g., diatoms), coccolithophores, and dinoflagellates, with their red algal-derived plastids. The transition from ancestral isogamy to oogamy was followed by three simultaneous reappearances of isogamy during the Cretaceous Period. These are concordant with a positive character correlation between parthenogenesis and isogamy. Our new brown algal timeline, combined with a knowledge of past environmental conditions, shed new light on brown algal diversification and the intertwined evolution of multicellularity and sexual reproduction.

INTRODUCTION

Brown algae (Phaeophyceae) are a lineage within the Heterokontophyta[1] (or photosynthetic stramenopiles), with plastids derived from a red algal endosymbiont.[2] Among heterokonts, brown algal diversity is second only to that of the diatoms, accounting for 46% of all non-diatom heterokonts (2,125 of 4,619 species, retrieved from AlgaeBase[3]). Brown algae are also morphologically diverse, ranging from small filaments to complex kelps (e.g., *Macrocystis*) that may become more than 60 meters long.[4] These algae vary not only in thallus morphological complexity but also in the differentiation of cell types, the establishment of a body plan, and the evolution of complex life cycles. Most brown algae undergo alternation of generations between a diploid sporophyte and haploid gametophyte (haplo-diplontic cycle); two exceptions are the Fucales and Ascoseirales, where the multicellular gametophyte stage has secondarily been lost (diplontic cycle).[5]

Brown algae are highly diverse in terms of morphology and life cycles, but there are shared characteristics that differentiate them from other photosynthetic heterokonts. The brown algae are one of the six eukaryotic lineages that show complex multicellularity, characterized by cell-to-cell adhesion, intercellular communication, different cell types, tissue differentiation, and a three-dimensional cellular organization.[6] Plasmodesmata, intercellular channels transporting nutrients or chemical signals, are present in all brown algae.[7] Moreover, sexual organs (i.e., plurilocular gametangia) are found in even the early-diverging brown algae.[8] By contrast, sister class to the brown algae, Schizocladiophyceae, lacks the components of the complex multicellularity (e.g., plasmodesmata and differentiation of sexual organs).[9] Therefore, to understand how complex multicellularity emerged,

Please cite this article in press as: Choi et al., Ordovician origin and subsequent diversification of the brown algae, Current Biology (2023), https://doi.org/10.1016/j.cub.2023.12.069

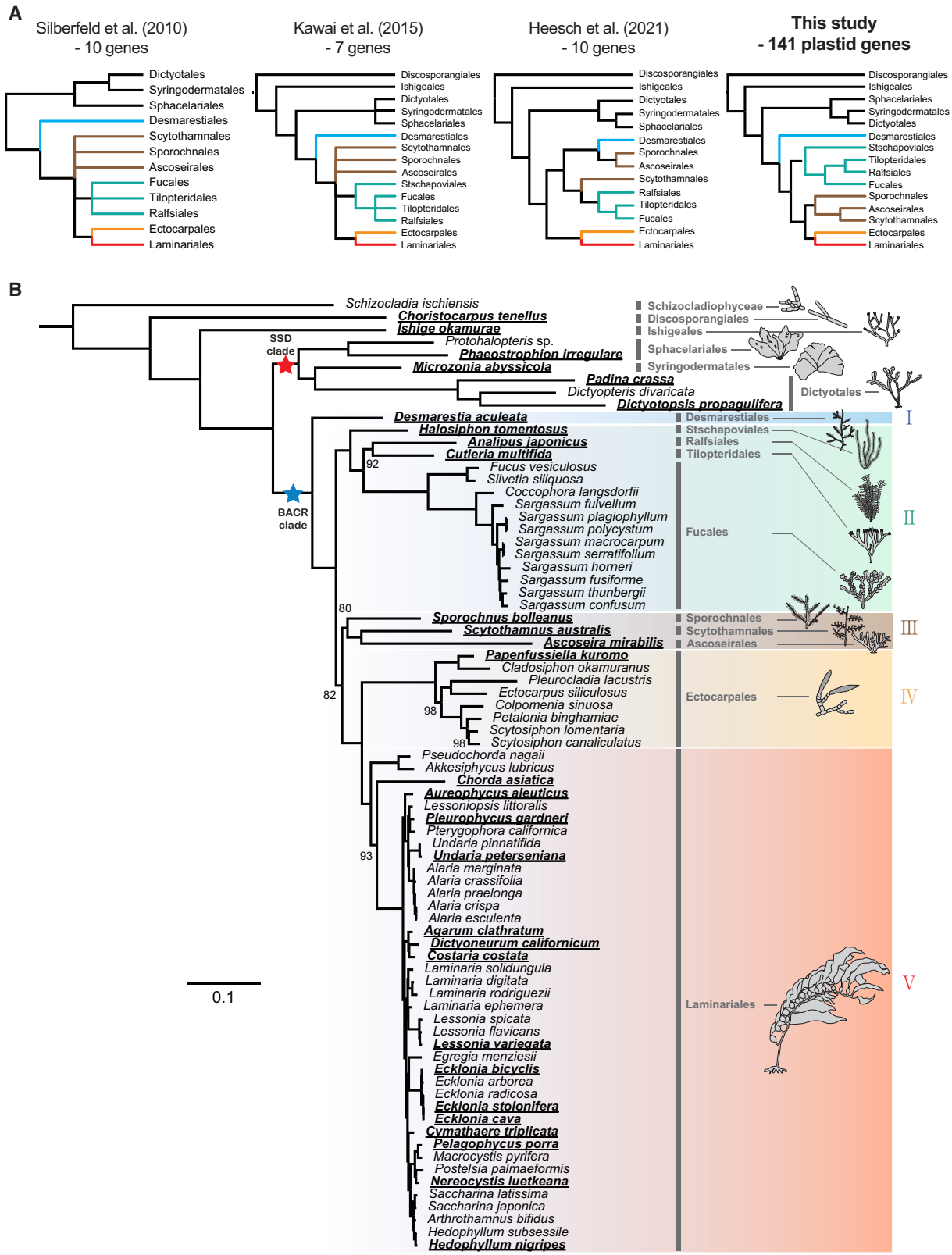

(legend on next page)

Please cite this article in press as: Choi et al., Ordovician origin and subsequent diversification of the brown algae, Current Biology (2023), https://doi.org/10.1016/j.cub.2023.12.069

it is crucial to know when intricate developmental morphogenesis (e.g., three-dimensional growth and cell differentiation) evolved.[10]

Brown algal gametes are produced within plurilocular gametangia. Brown algae differ in the extent to which they display gamete dimorphism, which can be classified into three types: isogamy (motile gametes of the same size), anisogamy (larger and motile female gametes), and oogamy (larger and nonmotile female gametes).[8] The evolution of "two sexes," more specifically, the evolution of anisogamy from the ancestral isogamy, has been discussed since Darwin formulated his sexual selection theory.[11] For example, asexually reproducing organisms can produce twice as many offspring as those that reproduce sexually, leading to the "cost of males" hypothesis.[12] Also, a zygote produced from isogametes includes the nucleus, cytoplasm, and organelles from both gametes. Conversely, the zygote produced from anisogametes includes only the cytoplasm and organelles from the larger female gamete, resulting in a loss of male gamete biomass and organellar genomes. Parker, Baker, and Smith (abbreviated as the PBS theory)[13] hypothesized that for any multicellular species, zygote survival requires enhanced nourishment for the embryo, leading to disruptive selection for dimorphic gametes (i.e., enlarged eggs and reduced sperm). The PBS theory was articulated for Volvocine green algae, which show a clear correlation between the degree of anisogamy and the extent of multicellularity.[14–16] Anisogamy has frequently been considered an evolutionarily stable condition in complex multicellular species, and, therefore, reversions to isogamy have not commonly been discussed.[13,17] In addition, it has been suggested that anisogamy led to "sex roles," i.e., a behavioral disparity between females and males (Bateman's principle).[13,18,19]

Although these theoretical positions are widely accepted, some brown algal lineages show evolutionary trends that contradict their predictions. For example, several derived brown algal orders have isogamous gametes (e.g., Ectocarpales, Syringodermatales, Ascoseirales, and Scytothamnales). In addition, pheromone-producing sedentary female gametes and actively swimming pheromone-detecting male gametes occur in these isogamous brown algae.[20] Therefore, isogamous brown algae seem to contradict the tenets of both the PBS theory and Bateman's principle. To elucidate why specific lineages are isogamous, a robust phylogeny, a geological timeline, and specific character correlations are necessary. A recent study tackled the question of sexual evolution in brown algae,[21] but the study suffers from insufficient data and technical problems that can foster misinterpretations.

In this study, we present a robust phylogeny and new timeline and use these to suggest a plausible scenario of brown algal evolution. We assembled 138 plastid genomes (hereafter termed plastomes; 118 ingroup [heterokontophytes] and 20 outgroup taxa [red algae, haptophytes, cryptophytes]), combining 35 new brown algal plastid genomes with 103 published plastomes. The dataset covers 16 of the 20 brown algal orders, representing most lineages of the brown algae (i.e., more than 99% of all brown algal species belong to these 16 orders). The four orders not included in this study are the Onslowiales, Nemodermatales, Asterocladales, and Phaeosiphoniellales, each of which has fewer than five described species.[3]

Using this organelle genome dataset, we investigated phylogenetic relationships of the brown algae, clarifying diversification within the brown algal crown radiation (BACR) clade, which remained unresolved in previous studies.[22–24] Within this robust phylogenetic framework, we found two major independent transitions from ancestral isogamy to oogamy, followed by three independent reversions from oogamy back to anisogamy or isogamy. Based on the new time estimation integrated with data covering main lineages of heterokontophytes and novel fossil constraints, we estimate the divergence time trajectories for brown algal diversification and gamete evolution. We discuss environmental factors that may have promoted these transitions.

RESULTS

Phylogenetic relationships within the brown algae

The contents of the 35 new plastid genomes (i.e., 20 newly sequenced and 15 newly assembled from NCBI Sequence Read Archive data) are shown in Data S1A. A brown algal maximum-likelihood tree was constructed using 141 concatenated protein-coding plastid genes, and the tree recovered the monophyly of the brown algae (Figure 1). From the close relative Schizocladiophyceae, the brown algae diverged into four major clades: (1) the Discosporangiales, (2) the Ishigeales, (3) the SSD clade (Sphacelariales, Syringodermatales, and Dictyotales), and (4) the BACR clade (BACR; 10 orders, see below). Within the BACR clade, five subclades showed successive diversifications with ultrafast bootstrap (BS) values of 100%, except for BACR III (BS > 80%): (clade I) Desmarestiales; (clade II) Stschapoviales, Ralfsiales, Tilopteridales, Fucales; (clade III) Sporochnales, Scytothamnales, Ascoseirales; (clade IV) Ectocarpales; and (clade V) Laminariales. Inter-ordinal branches within/between the clades were highly supported (BS 90%–100%), except the monophyly of Scytothamnales + Ascoseirales and Sporochnales (BS 80%) and the monophyly of BACR clades III + IV + V within the BACR (BS 82%) (Figure 1B).

To test whether similar gamete types share a common ancestor, we conducted an alternative tree topology test that forced the monophyly of isogamy (Scytothamnales + Ascoseirales + Ectocarpales) and oogamy (Dictyotales + BACR clade), respectively. This test showed that the monophyly of both Scytothamnales + Ascoseirales + Ectocarpales and Dictyotales + BACR clade were rejected (Table 1), refuting

Figure 1. Phylogenetic studies of the brown algae

(A) Evolving topology of the brown algal orders, with increasing molecular markers and taxa. Branches whose bootstrap supports are less than 75% are treated as polytomies (Heesch et al.[21] used Bayesian posterior probability). Note the gradual increase in resolution of brown algal crown radiation (BACR) diversifications. (B) A maximum-likelihood phylogenetic tree of brown algae based on plastome amino acid sequences (141 genes). The two major clades of the brown algae, SSD (Sphacelariales, Syringodermatales, and Dictyotales) and BACR clades, are marked with red and blue stars. Five successive diversifying lineages of the BACR clade are specified with I–V labels. The 29 brown algal species whose plastomes are newly assembled and annotated are emboldened and underlined. Bootstrap support values that are not 100% are shown on the branches.

See also Figures S1 and S2 and Data S1.

Please cite this article in press as: Choi et al., Ordovician origin and subsequent diversification of the brown algae, Current Biology (2023), https://doi.org/10.1016/j.cub.2023.12.069

Table 1. Results of tree topology tests for alternative topological hypotheses

Alternative tree topology	bp-RELL	KH	SH	ELW	AU
Scytothamnales + Ascoseirales + Ectocarpales	0	0	0	0	0
Scytothamnales + Sporochnales	0	0	0.0203	0	0
Ascoseirales + Sporochnales	0	0.0001	0.0831	0	0.0010
Dictyotales + BACR clade	0	0	0	0	0
Sphacelariales + Dictyotales	0.0031	0.0138	0.0996	0.0304	0.0766
Sphacelariales + Syringodermatales	0.0872	0.085	0.266	0.0867	0.102

The tree topology column indicates the taxa that are treated as monophyletic in the alternative tree topologies that were tested. Values less than 0.0001 were treated as 0. bp-RELL, bootstrap proportion test using resampling estimated log-likelihoods; KH, weighted Kishino-Hasegawa test; SH, weighted Shimodaira-Hasegawa test; ELW, expected likelihood weight test; AU, approximately unbiased.

the possibility of the single origin of isogamy. However, Sphacelariales + Syringodermatales and Sphacelariales + Dictyotales were not significantly rejected, leaving the possibility of different evolutionary patterns within the SSD clade (Table 1).

To further test the reliability of the plastome tree, three other phylogenetic reconstructions were attempted with the following modifications: (1) nucleotide tree: the tree constructed with plastome nucleotide sequences was generally congruent with the amino acid tree. The only supra-ordinal topological difference was found within the SSD clade (monophyly of Sphacelariales + Syringodermatales, in contrast to the monophyly of Syringodermatales + Dictyotales in the amino acid tree), but with less support for Sphacelariales + Syringodermatales (BS 99%) and SSD monophyly (BS 92%) than the amino acid tree. There were also some topological differences among kelp species (e.g., position of *Egregia menziesii* and *Undaria* spp.), all of which occurred at an infra-ordinal level. (2) Accumulation of genes that satisfied phylogenetic assumptions: tests of symmetry for each plastid gene showed that 96.45% of the genes (136 among 141 genes) passed the tests, meaning the genes passed a statistical threshold (>0.05 maximum symmetry p value) of not violating constant sequence variation and substitution assumptions. We arranged 141 genes in a row of increasing p values from the symmetry test and then accumulated five genes sequentially. The result showed that the topological order of BACR clades was recovered after an accumulation of 50 genes, and with the further accrual of genes that are more than 65 genes, the topology was sustained with a BS > 90% (Figure S1), indicating that our gene selection strategy reproduced the same topology based on all genes. (3) A multispecies coalescent tree construction: The multispecies coalescent tree, reconstructed with ASTRAL-III software, showed two order-level topological differences when compared with the maximum-likelihood (ML) 141 amino acid supermatrix tree (Figure S2), i.e., the monophyly of SSD clade and the paraphyly of the BACR clade III (Sporochnales, Scytothamnales, and Ascoseirales). All these tests suggest the robustness of current plastome tree.

Divergence time estimation of the photosynthetic stramenopiles

A maximum-likelihood tree constructed using protein sequences of the 141 plastid genes was used as a backbone tree for the divergence time estimation with eight fossil constraints (Table 2). The estimated divergence times are shown in Figure 2 and Table 3. There were very few differences with respect to the choice of genes, protein model (chloroplast reversible [cpREV] and Whelan and Goldman [WAG]), and fossil calibration schemes; most differences were less than 10 Ma in important nodes (Table 3). The only factor that led to notable discrepancies between time estimations was the clock model (uncorrelated vs. autocorrelated) employed. The estimated time of crown heterokontophytes was relatively similar (ca. 770–780 Ma in the uncorrelated clock result and ca. 800–810 Ma in the autocorrelated clock result). However, there was more than 100 Ma of estimation gap between our two clock models for brown algal origins (uncorrelated: 435–455 Ma; autocorrelated: 595–600 Ma; see detail in Table 3).

To check which clock model (uncorrelated or autocorrelated) is more suitable for the time estimation of heterokont algal divergences, we examined two factors related to the performance of the clock model: the extent of autocorrelation of the phylogenetic tree and robustness with respect to different fossil

Table 2. Fossil calibrations used for the time estimation

Fossils	Nodes	Minimum	Maximum	References
Julescraneia	*Pelagophycus* + *Nereocystis*	13 Ma	–	Parker and Dawson[25]
Paleocystophora, *Paleohalidrys*	Sargassaceae (*Coccophora* + *Sargassum*)	13 Ma	–	Parker and Dawson[25]
Padina	Dictyotales (*Padina* + *Dictyotopsis*)	100 Ma	–	Rajanikanth[26]
Tetraparma aff. *Mirabilis*	Parmales (Parmales sp. + *Tetraparma*)	66 Ma	–	Abe and Jordan[27]
Helmet-shaped diatom epivalve	Diatoms (*Leptocylindrus* + *Proboscia*)	139 Ma	240 Ma	Harwood et al.[28] and Behrenfeld et al.[29]
Eunotia-like raphe-bearing diatom	stem group of raphid diatoms (*Synedra* + *Eunotia*)	82 Ma	139 Ma	Siver and Velez[30]
Chrysophyceaen cysts	Chrysophyceae (*Poterioochromonas* + *Chromulina*)	228 Ma	–	Zhang et al.[31]
Mallomonas W1	Synurales (*Mallomonas* + *Synura*)	83 Ma	228 Ma	Siver[32]

Please cite this article in press as: Choi et al., Ordovician origin and subsequent diversification of the brown algae, Current Biology (2023), https://doi.org/10.1016/j.cub.2023.12.069

CellPress

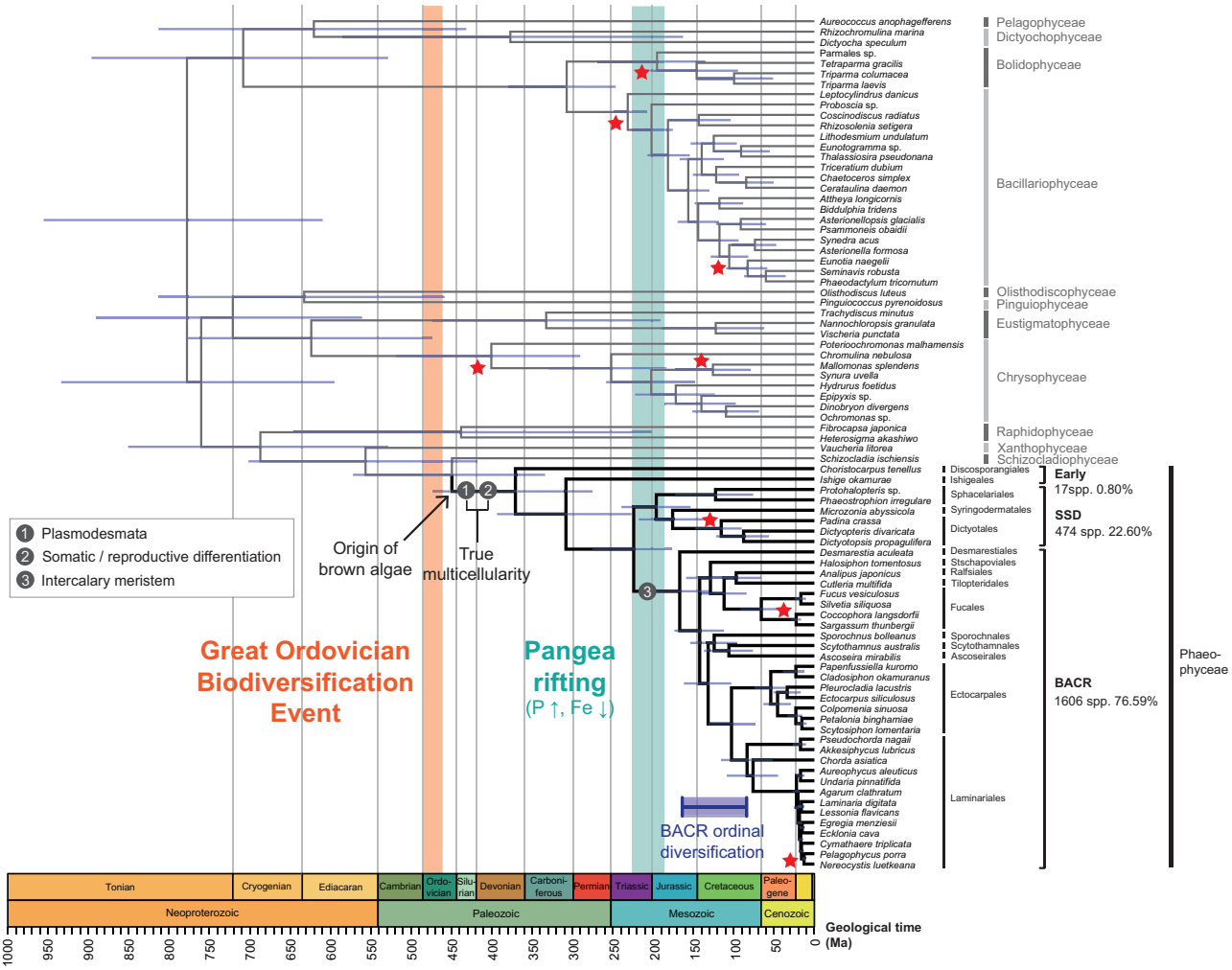

Figure 2. Divergence time of the photosynthetic stramenopiles

Bayesian divergence time estimation of the brown algae using the 77 plastid protein sequences and eight fossil calibrations (marked with red stars). For more information of each fossil, refer to Table 2 and Figure S5. Blue bars on the nodes show 95% HPD intervals of the node ages. The Great Ordovician Biodiversification Event (GOBE) is shown as an orange box and Pangea rifting as a blue box.
See also Figures S3–S5 and Data S1.

calibration schemes. The extent of autocorrelation among distinct lineages was analyzed with CorrTest,[33] providing a metric called CorrScore, where if the score is close to 0, there are few signals of autocorrelation, whereas if close to 1, a high level of autocorrelation is expected. The CorrScore of total heterokont lineages was an ambiguous 0.576. However, there are striking differences among different lineages of heterokonts. In the diatom lineage (S3 clade), CorrScore was 0.951, which means evolutionary rates were highly correlated. By contrast, in the chrysophyte-related lineage (S2 clade) and the brown algal lineage, CorrScores were 0.001 and 0.124, respectively, strongly suggesting uncorrelated evolutionary rates within these lineages. The differences in evolutionary rate per unit time among lineages are shown in Figure S3. Moreover, the robustness of time estimation with respect to clock models was tested by serially discarding calibration points. The result (Figure S4A) shows that when each of eight fossil calibrations was discarded, respectively, differences in the mean age of the uncorrelated clock were less than those of the autocorrelated clock in most cases. One node that showed more robustness of the mean difference in the autocorrelated clock model is *Nereocystis-Pelagophycus*, which is the most recent calibration node (13 Ma) among the fossil constraints used. We also compared Cohen's d, the summary statistic of effect size between distributions. It showed that in the four nodes (Raphid diatom, Chrysophyceae crown, Synurales, and Dictyotales), the uncorrelated clock results had significantly smaller Cohen's d statistic than the correlated clock results (0.18 vs. 2.13, 0.14 vs. 0.91, 0.24 vs. 0.87, and 0.74 vs. 1.39, respectively; Figure S4A). The independent clock results were also stable when estimating the age of the brown algal origin node. Except for one case (i.e., excluding the crown diatom fossil constraint), mean estimation values for a brown algal origin using independent clock priors were ca. 400–450 Ma across different calibration schemes. By contrast, the correlated clock prior results showed about twice more variation (ca. 500–600 Ma, Figure S4B).

Please cite this article in press as: Choi et al., Ordovician origin and subsequent diversification of the brown algae, Current Biology (2023), https://doi.org/10.1016/j.cub.2023.12.069

Table 3. Bayesian time estimation results

Clock model	Uncorrelated						Autocorrelated	
Protein model	cpREV					WAG	cpREV	WAG
Fossil calibrations	Soft bound				Hard bound	Soft bound		
Number of genes	77 genes (total)	60 genes	40 genes	20 genes	77 genes (total)			
Time estimation of crown group (Ma)								
Heterokontophyta	777.84	777.30	770.21	782.99	784.56	731.74	811.00	801.25
Diatoms	231.40	231.54	231.30	231.66	229.47	230.79	231.10	231.08
Chrysophyceae	400.53	400.58	397.57	404.12	404.19	383.46	346.02	341.43
Schizo + Phaeo	449.41	448.88	445.95	452.24	455.80	435.06	602.06	595.04
Phaeophyceae	370.67	370.34	368.48	372.88	375.52	361.44	545.52	538.37
Ishige + SSD + BACR	308.00	307.80	306.89	309.98	312.69	302.98	495.77	489.04
SSD + BACR	223.99	224.13	223.85	225.21	227.78	224.23	402.07	396.99
SSD	195.98	196.08	195.93	197.04	199.65	196.09	357.73	352.58
BACR	166.96	167.42	166.83	167.40	169.36	168.49	346.45	340.80
BACR II + III + IV + V	142.23	142.67	142.24	142.43	144.12	142.99	312.31	305.46
BACR III + IV + V	131.74	132.16	131.77	131.89	133.42	133.08	298.13	292.26
BACR IV + V	102.74	103.05	102.82	102.71	104.07	104.13	255.13	249.38
BACR V (Laminariales)	83.44	83.53	83.58	83.39	84.40	82.24	231.51	223.40
Dictyotales	115.50	115.71	115.76	115.99	119.44	115.33	138.70	137.24
Fucales	65.81	66.10	65.86	65.90	66.95	66.63	134.28	134.23
Ectocarpales	54.08	54.27	54.02	54.25	54.77	55.75	135.60	133.34

Following the time estimation results using 77 all-conserved protein sequences with uncorrelated clock, cpREV protein model, and soft bound fossil calibration, the root mean age of the crown heterokontophytes was estimated as 777.84 Ma (95% highest posterior density [HPD, 609.58–955.63 Ma]). The origin of the brown algae—that is, the divergence between the Schizocladiophyceae and the Phaeophyceae—is estimated to have occurred during the Ordovician Period (449.41 Ma [333.85–572.02 Ma]). Within the Phaeophyceae, the divergence age of *Choristocarpus tenellus* (Discosporangiales) was estimated to have occurred in the Devonian Period (370.67 Ma [274.98–474.06 Ma]). The Ishigeales diverged during the Late Carboniferous Period (308.00 Ma [226.65–393.42 Ma]), whereas the SSD and BACR clades diverged in the Triassic Period (223.99 Ma [177.16–274.90 Ma]). The SSD-BACR divergence occurred almost simultaneously with the onset of diatom divergence (231.40 Ma [207.34–248.53 Ma]). The SSD root was estimated as 195.98 Ma ([153.49–239.28 Ma], Jurassic Period) and BACR root as 166.96 Ma ([130.19–205.51 Ma], Jurassic Period), respectively. The diversification of basal brown algal orders (from Discosporangiales to SSD + BACR) occurred in an interval of over 150 Ma (ca. 371–224 Ma), whereas the diversification of the BACR orders occurred in a much shorter geological interval of 84 Ma from (ca. 167–83 Ma) (Figure 2; Table 3), suggesting more rapid radiation in this lineage.

Given questions concerning the phylogenetic affinity of *Miaohephyton*, which has conceptacle-like structures and intercalary meristem, we estimated the brown algal divergence time with this fossil constraint (BACR-SSD at 550 Ma; Figure S5A). In this case, the estimated (Figure S5A) age for the SSD-BACR (349.66 Ma [95% HPD: 251.35–465.89 Ma]) is far younger than the minimum soft bound of the fossil *Miaohephyton* (550 Ma), indicating that *Miaohephyton* may not be interpreted correctly as a phaeophyte. Without diatom crown fossil calibration, estimated ages were increased overall (compare Figures 2 and S5B), although we must bear in mind that, along with coccolithophorids (Haptophyta), diatoms are the heterokont lineage best constrained by fossil occurrences. In this case, the age of crown heterokontophytes was estimated as 965.93 Ma (728.96–1,231.03 Ma), ca. 190 Ma older than the result with the diatom crown fossil calibration (777.84 Ma [609.58–955.63 Ma]). The origin of brown algae was estimated as 549.29 Ma (391.59–719.62 Ma). We also estimated divergence time without maximum constraints for two fossils (*Mallomonas* [228 Ma] and *Eunotia*-like raphe [139 Ma]). We found that the time differences for the fossil nodes were less than 5 Ma (104.34 vs. 105.56 Ma at the *Eunotia*-like raphe node; 121.84 vs. 125.84 Ma at the *Mallomonas* node). The age estimation for the origin of brown algae was ca. 4 Ma different (445.47 vs. 449.41 Ma). The results are shown in Figure S5C.

Ancestral state, transitions, correlation, and comparison of characters

The ancestral states of phaeophyte gametes (i.e., isogamy, anisogamy, and oogamy) were estimated using maximum-likelihood ancestral state construction (pie charts in Figure 3A). The major ancestral gamete states in the brown algal root were estimated to be isogamy with a high proportion of oogamy (isogamy: 48.47%, anisogamy: 13.97%, oogamy: 37.56%). This correlates well with the gamete state of the early-diverging lineages (i.e., Discosporangiales, Ishigeales, Sphacelariales, and Syringodermatales), all of which are isogamous (Figure 3A). The proportion of isogamous species decreased by more than 20% only two times, (1) in the ancestor of the BACR clade (from 34.93% to

Please cite this article in press as: Choi et al., Ordovician origin and subsequent diversification of the brown algae, Current Biology (2023), https://doi.org/10.1016/j.cub.2023.12.069

CellPress

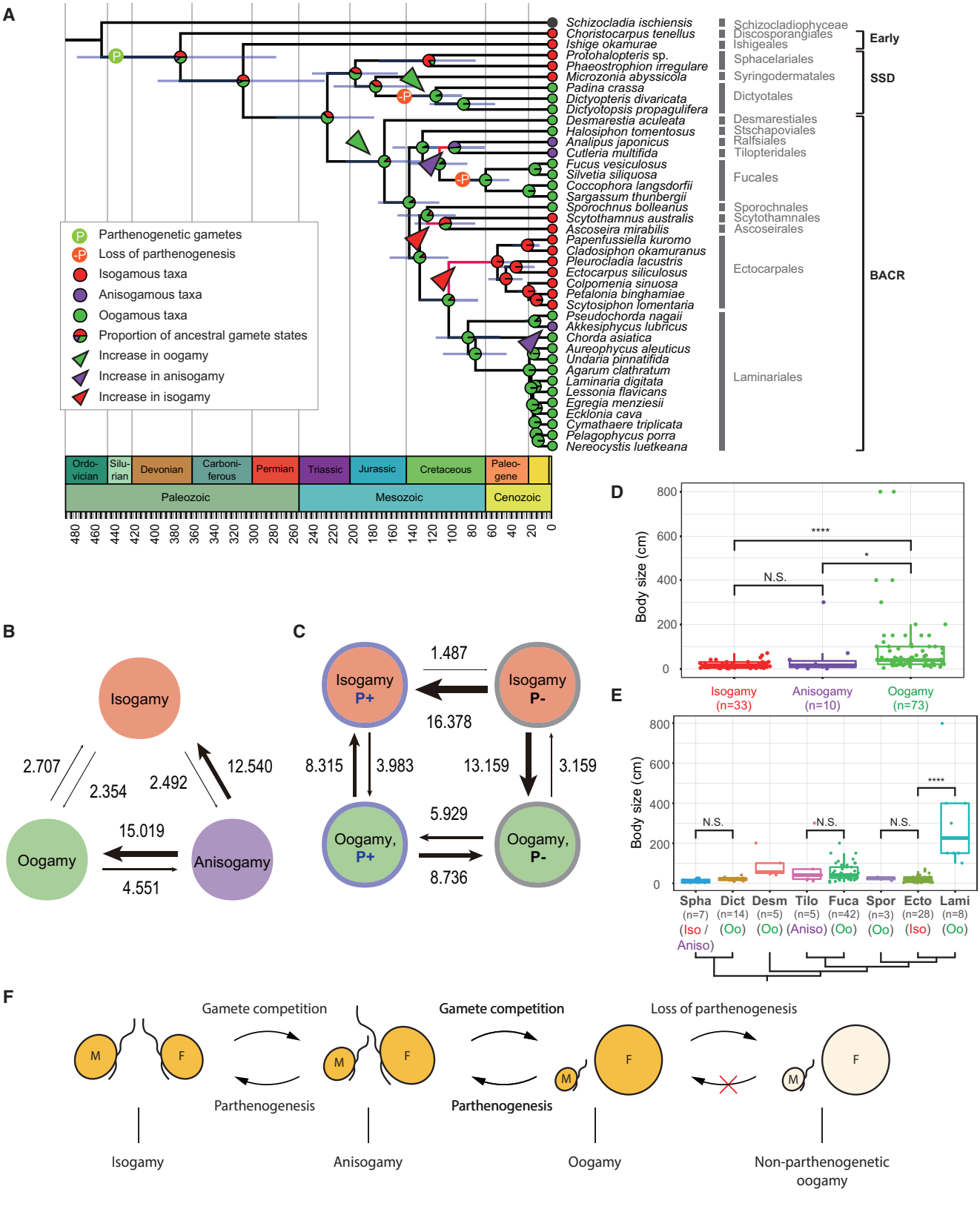

(legend on next page)

Please cite this article in press as: Choi et al., Ordovician origin and subsequent diversification of the brown algae, Current Biology (2023), https://doi.org/10.1016/j.cub.2023.12.069

10.88%), and (2) in the ancestor of the Dictyotales (from 38.04% to 4.79%), and these two instances indicate a transition from ancestral isogamy to oogamy (see two green triangles in Figure 3A). We tested for the occurrence of a single transition in the hypothetical common ancestor of the oogamous BACR and the Dictyotales using an alternative tree topology test. The alternative tree topology test significantly rejected this single transition topology ($p < 0.0001$, Table 1), thereby confirming the two independent transitions from isogamy to oogamy in the ancestors of BACR and the Dictyotales.

Contrary to the brown algal root, the ancestral state of the BACR clade was dominated by oogamy (isogamy: 10.88%, anisogamy: 1.08%, oogamy: 88.04%). Within the BACR clade, brown algal species are predominantly oogamous, with less than 20% being isogamous or anisogamous. In the BACR, decreases in the proportion of oogamy by more than 20% and simultaneous increases in proportion of isogamy were observed twice, within the Ectocarpales and Scytothamnales-Ascoseirales (see red triangles in Figure 3A). The proportion of isogamy increased from 11.65% in the Ectocarpales-Laminariales ancestor to 99.07% in the ancestor of Ectocarpales and from 14.24% in the Sporochnales-Scytothamnales-Ascoseirales ancestor to 53.33% in the Scytothamnales-Ascoseirales ancestor. These transitions to isogamy occurred independently because the alternative tree topology tests significantly rejected a single origin of isogamy for the Scytothamnales-Ascoseirales and the Ectocarpales ($p < 0.0001$, Table 1).

We found two cases where anisogamy was derived from oogamous ancestors. The first was from 89.97% of oogamy in Fucales-Ralfsiales-Tilopteridales ancestor to 49.51% of anisogamy in the Ralfsiales-Tilopteridales ancestor (see purple triangles in Figure 3A). The second was from 89.19% of oogamy in the *Pseudochorda nagaii-Akkesiphycus lubricus* ancestor to anisogamy in *A. lubricus*. However, the BayesTraits analysis for the character transition rate (Figure 3B) shows that anisogamy likely changed to either isogamy (12.540) or oogamy (15.019) rather than vice versa (2.492 and 4.551). Therefore, the anisogamous states in Ralfsiales, Tilopteridales, and *Akkesiphycus lubricus* (Laminariales) were unstable evolutionary conditions. Furthermore, the direct transition rates from isogamy to oogamy (2.354) and from oogamy to isogamy (2.707) are low compared with those where anisogamy was an intermediary stage, i.e., (15.019 and 12.540), respectively. Thus, the transition between isogamy and oogamy generally included an intermediary anisogamy stage.

The impact of different transition models (ER, equal rates; SYM, symmetric rates; and ARD, all rates different) was tested, and the results are shown in Data S2A and S2B. Log-likelihood tests failed to reject the ER model (ER vs. SYM: $p = 0.1795$, ER vs. ARD: $p = 0.1941$). The ER and SYM models alike supported an isogamous ancestor, but the ARD model resulted in an oogamous ancestor. For the ARD model, the transition rate from isogamy to oogamy was calculated as 0, which was due to an overparameterization that occurred in the low-to-medium size (tip number: 5∼95) trees.[34]

We tested an alternative interpretation of gamete types by assuming the Laminariales were an anisogamous lineage, i.e., some members have flagellated egg cells and the size differences between male and females are less pronounced than for other brown algae.[35] The results show that the major conclusions remain the same as before: (1) an isogamous root, (2) an oogamous BACR ancestor, and (3) a reversion to (an)isogamy in three independent BACR lineages (Data S2B).

We also estimated the brown algal ancestral state for meristematic growth sites (apical or intercalary; Figure S6A). The result shows that, for all brown algae, an apical growth pattern was ancestral; however, for the ancestor of the BACR clade, an intercalary growth pattern was ancestral. Furthermore, there were two independent reversions to the apical growth pattern—within the Fucales and within the Scytothamnales + Ascoseirales.[35] The estimated ancestral state for parthenogenesis (parthenogenetic or non-parthenogenetic; Figure S6B) shows that parthenogenetic gametes were ancestral for most brown algae, but some oogamous lineages lost the parthenogenetic pathway (Dictyotales, Fucales, and some species of Laminariales).

We performed a correlation test of two binary characters (i.e., gamete states and parthenogenetic ability) using BayesTraits (see Figure 2C). Log Bayes factor, which was calculated from log marginal likelihoods of independent and dependent evolutionary models, was 5.941 (interpreted as "strong evidence ($BS > 5$)" for dependent evolution between gamete states and parthenogenetic ability[36]). A continuous-time Markov model analysis of the two discrete traits, when considering their dependence, showed two anti-directional flows of gamete states; when parthenogenetic ability was present in the gametes (P+), oogamy to isogamy flow was dominant (8.315) compared with isogamy to oogamy (3.983). By contrast, in a non-parthenogenetic condition (P−), isogamy to oogamy movement was pervasive (13.159) compared with oogamy to isogamy (3.159). When there was a fixed isogamous gamete state, the parthenogenetic state was highly preferred (16.378) to the non-parthenogenetic state (1.487), but when there was a fixed oogamous gamete state, the transition rate from parthenogenetic to non-parthenogenetic (8.736) was greater than vice versa (5.929).

Figure 3. Gamete transitions in the brown algae

(A) Timeline of the brown algal gamete transitions. The unit of time is Ma. The full circles of the three characters (red circles: isogamy, purple circles: anisogamy, green circles: oogamy) are assigned on the tips of the phylogeny, and the proportions of the estimated gamete states are shown on each node as a pie chart. The ancestral branches where reversions to isogamy occurred are shown as red lines.

(B) The transition rates among the three gamete traits. Width of each arrow mirrors the extent of the transition rate.

(C) The correlation between two discrete states, gamete type (isogamy and oogamy), and parthenogenetic ability (parthenogenetic and non-parthenogenetic). P+ refers to parthenogenetic and P− non-parthenogenetic. Width of each arrow mirrors the extent of the transition rate.

(D) Comparison of maximum thallus size between brown algal groups with different types of gametes.

(E) Comparison of maximum thallus size between different phylogenetic groups (orders) of brown algae. N.S.: not significant ($p > 0.05$), *$0.01 < p < 0.05$, ****$p < 0.0001$.

(F) The schematic model of gamete evolution. Dark yellow gametes indicate parthenogenetic gametes, and light yellow non-parthenogenetic gametes.

See also Figure S6 and Data S1 and S2.

Please cite this article in press as: Choi et al., Ordovician origin and subsequent diversification of the brown algae, Current Biology (2023), https://doi.org/10.1016/j.cub.2023.12.069

The maximum thallus size of brown algal species was compared according to their gamete types and orders (Figures 3D and 3E). When the species were arranged according to their gamete types, without considering phylogenetic relationships, the body size of oogamous species was significantly larger than anisogamous ($p < 0.05$, Wilcoxon test) and isogamous ($p < 0.0001$, Wilcoxon test) species (Figure 3D). However, when sister orders with different gamete types were compared, generally there was no significant difference between the phylogenetically related orders (i.e., isogamous/anisogamous Sphacelariales-oogamous Dictyotales, anisogamous Tilopteridales-oogamous Fucales, isogamous Ectocarpales-oogamous Sporochnales; Figure 3E). One exception was isogamous Ectocarpales-oogamous Laminariales ($p < 0.0001$, Wilcoxon test).

DISCUSSION

Divergence time estimations for brown algae

We estimated the Phaeophyceae root age by calibrating with eight fossil constraints. The result shows the mean age of phaeophycean origin as 449.41 Ma (95% HPD: 333.85–572.02 Ma, Ordovician Period), which is ca. 1.8–2.8 times older than several previously published estimates (e.g., ~183 Ma [Jurassic Period],[22] ~250 Ma [Permian-Triassic boundary],[24] ~190 Ma [Jurassic Period],[21] ~160 Ma [Jurassic Period][37]). These discrepancies in divergence time are likely due to three reasons. First, we removed the outdated secondary root constraint of the brown algae. Three former time estimation studies[21,22,24] used a secondary calibration for determining the phaeophycean root (155 Ma[38]). However, the use of 155 Ma as the brown algal root prior has some limitations. The age estimation of the brown algal root was obtained with only a single gene (SSU rRNA) and used the constraints of a single diatom fossil.[38] Moreover, the brown root age was estimated using a simple regression of neighbor-joining tree branch lengths, which is much more simplistic than current time estimation methods that consider rate heterogeneity across lineages.[39] Thus, we used uniform priors and assigned a soft bound to the minimum and maximum ages. Second, we used broader taxon-sampling comprising other lineages of photosynthetic heterokonts and early-diverged brown lineages (i.e., Discosporangiales and Ishigeales) that some of the previous studies did not include.[22,37] Third, we incorporated new fossil calibrations ranging from kelps to other heterokontophytes. Taken together, these should provide a better approximation of the divergence time for the brown algae.

Interestingly, time estimation in this study is generally supported by several recent studies that have used sophisticated relaxed clock estimation methods with numerous species covering major eukaryotic phyla (109 in Parfrey et al.[40] and 733 in Strassert et al.[41]), included Phanerozoic and Proterozoic fossils (23 in Parfrey et al.[40] and 33 in Strassert et al.[41]), and used multiple genes (15 protein-coding genes in Parfrey et al.[40] and 320 in Strassert et al.[41]). Consistent with our estimates, these studies suggest that the divergence of the Heterokontophyta from its sister lineages occurred at ca. 800 Ma (Cryogenian Period).[40,41]

The time estimation results in this study also have some limitations. This study has no calibration points within the deep inter-ordinal nodes. The scarcity of the early brown algal fossils reflects the absence of mineralized parts, which aid in preservation, and morphological convergences among early-diverging macroalgal morphologies.[42] To establish a more robust timescale for the brown algal diversification in future studies, fossils from early-diverged brown algal lineages are essential for time calibration. Nonetheless, based on our results, we anticipate that the early-diverged brown algae during the Paleozoic Era might have been uniseriate filaments (e.g., *Choristocarpus* in Discosporangiales), perhaps only identifiable by seldom-preserved morphological characteristics such as plasmodesmata, apical growth, and reproductive organs.

Establishment of complex multicellularity and later diversification

Time estimations for the origin of brown algae—in other words, the origin of cell-to-cell communication (i.e., plasmodesmata) and differentiation of somatic and reproductive cells—fall between the late Ordovician and Devonian Periods (Figure 2; Table 3). Plasmodesmata act as channels for directed intercellular transport of nutrients and regulatory proteins into neighboring cells, enabling three-dimensional patterns of cell differentiation.[7,43] Two major ecological and environmental changes occurred during the time interval when complex multicellularity emerged in brown algae.

Ecologically, predators (herbivory) may facilitate a transition from a unicellular to a multicellular form, as supported by experimental studies.[44–46] From the systematic analysis of fossil remains, most macroalgal fossils before the Ordovician Period had delicate branches (<2 mm), with only a minor admixture of more complex parenchymatous forms.[47] By contrast, during the Ordovician Period complex morphotypes of macroalgae (coarsely branched [>2 mm] or monopodial branched patterns)—some with mineralized skeletons—diversified within both green and red algae.[47–49] These fossil distributions are consistent with our estimated time for the origin of brown algae and suggest that multiple clades responded in similar ways to increasing predation pressure associated with the marked diversification of marine invertebrates termed the Great Ordovician Biodiversification Event (GOBE)[48] (see Figure 2).

Environmentally, the rise of oxygen concentration may be conducive to complex multicellularity. Early animal diversification has commonly been linked to increasing levels of oxygen in marine surface waters,[49] and some evidence indicates that oxygenation increased further during the Ordovician Period.[50] By the Devonian Period, ocean basins were largely oxygenated.[51,52] Thus, macroalgal radiation occurred amidst physical as well as biological and environmental changes. Oxygen is used in a variety of developmental programs in many eukaryotic lineages, including animals, land plants, and algae. Relative concentrations of reactive oxygen species (ROS) trigger developmental pathways that are specific to tissues or organs.[53] Brown algae adjust ROS concentration to construct various developmental patterns such as embryogenesis or rhizoid cell growth.[54,55]

Renewed divergence of brown macroalgae began during the mid-Triassic Period, and this was followed by a Cretaceous diversification (Figure 2; Table 3). The common ancestor of most brown algal species (99.19% of species in the BACR + SSD clade) started to diversify from 223.99 Ma, after

Please cite this article in press as: Choi et al., Ordovician origin and subsequent diversification of the brown algae, Current Biology (2023), https://doi.org/10.1016/j.cub.2023.12.069

the end-Permian mass extinction and coincident with Pangea rifting. End-Permian extinction appears to have decimated Archaeplastid lineages that had dominated primary production in Paleozoic oceans, creating permissive ecology for the expansion of other clades.[56] Moreover, in the robustly ventilated oceans of the early Mesozoic Era, iron limitation may have favored chlorophyll a+c algae with their relatively low Fe requirement[57]; along with phaeophytes, coccolithophorids, diatoms, and photosynthetic dinoflagellates radiated in Mesozoic oceans. Also, after the mass extinction, the supercontinent Pangea started to break up about 230 Ma (Triassic Period).[58] Pangea rifting would have impacted algal ecosystems in two different ways. First, the area of coastal habitats increased due to continental break-up. Second, Pangea break-up may have increased nutrient fluxes into the seas, again facilitating the expansion of algal groups with red-derived plastids.[59]

Gamete transitions and impact of parthenogenesis

Since the advent of the classical PBS theory, oogamy has been regarded as the final gamete stage necessary for the further development of large, complex multicellular organisms.[13,19,57] The size of mature organisms has frequently been related to development of anisogamy from isogamy.[13,16] Additionally, the relationship of oogamous reproduction with other multicellular characteristics, such as cell-to-cell communication and transport of signals or nutrients, has been studied. Volvocine green algae evolved a cytoplasmic bridge system, through which molecular signals and nutrients could be transmitted between neighboring cells.[60] In lineages of the Streptophyta, oogamous reproduction and plasmodesmata are highly correlated, typically with simultaneous gain or loss. For instance, charophycean green algae acquired plasmodesmata and oogamous reproduction, but zygnematophycean algae secondarily lost both characters.[61,62] Cell-to-cell communication has been regarded as a prerequisite for differentiation of somatic and reproductive cells (i.e., division of labor) and, in turn, to the evolution of oogamy.[63]

It seems, however, difficult to apply this evolutionary trend to the case of brown algae. Generally, thallus size is not significantly different between closely related taxa with different gamete types (Figure 3D), the one exception being the Ectocarpales-Laminariales (oogamous Laminariales is significantly larger than isogamous Ectocarpales). In this case, however, it is more reasonable to interpret this as a kelp-specific innovation, not due to gamete transition per se, because there is no significant difference in thallus size between oogamous Sporochnales and isogamous Ectocarpales (Figure 3E). Also, brown algae evolved as complex multicellular organisms with plasmodesmata, somatic/reproductive cell differentiation, and multidirectional cell division (Figure 2) from the common ancestor of the Schizocladiophyceae and Phaeophyceae, which lacked plasmodesmata.[9] Unlike animals, land plants, and many green lineages (but excluding the isogamous ulvophycean green algae[64,65]), isogamy has persisted in brown algae for more than 400 million years (Figure 3). This prolonged isogamous history runs counter to the hypothesis that isogamy is not sustainable in complex multicellular organisms.[13,65]

There have been many theoretical studies exploring the conditions for anisogamy evolution, but they do not readily explain isogamous multicellular species.[13,17,57] Parthenogenesis, as suggested by a recent modeling study,[64] may influence the persistence of isogamy in brown algae. Distinct from most other eukaryotic lineages, the capacity for parthenogenesis is ancestral in the brown algae[8,21] (Figure S6B). All isogamous and anisogamous species, and even some oogamous taxa, can be parthenogenetic (except for some lineages that secondarily lost parthenogenetic ability in Fucales, Dictyotales, and some kelp species; Figures 3A and S6B[66]). If a parthenogenetic cycle is present in both sexual types of gametes and frequently activated, equal-sized gametes (i.e., isogamy) are likely to be favored over oogamy. Furthermore, in the transition from anisogamy to isogamy, resources are allocated to increase the size of smaller gametes to achieve a minimum size for survival.[13,57] Environmental changes over geological time likely contributed to sexual/asexual transitions and to gamete type transitions; however, no studies have specifically tested this possibility. Here, we examine possible selective forces acting on gamete evolution.

The modeling study that considered the parthenogenetic life cycle of isogamous species[64] argued that evolution from isogamy to oogamy involves two scenarios: (1) loss of parthenogenesis and (2) severe gamete competition.[64] In the brown algal orders that lost parthenogenetic ability (i.e., Dictyotales and Fucales, Figure 3A), species show oogamy without exception. Moreover, in our time estimation analysis (Figure 3A), we predict that ancestral isogamy diversified into anisogamy and oogamy during or after the Triassic and Jurassic Periods. A variety of factors may help to explain why this diversification happened when it did. First, there was a transition of photosynthetic dominance from Archaeplastida to chlorophyll-c containing algae, arguably related in part to increasing phosphorus availability[67] and possibly leading to dense populations and gamete competition. Second, there emerged innate and environmental conditions that facilitated mating success. The brown algal receptacle (i.e., a conceptacle-bearing reproductive organ in Fucales and Scytothamnales-Ascoseirales), which controls and synchronizes gamete release during the favorable conditions,[68] first appeared in the Cretaceous Period (Figure S6A) and may have greatly increased the survival rate of gametes.

Among species that are isogamous, it is probable that parthenogenesis played a role in maintaining or reversing to isogamy.[64] Parthenogenesis would be ecologically advantageous in rapidly changing or highly disturbed environments because populations could be successfully established without mating, providing an advantage over sexually reproducing populations.[69] The environmental factors that activate either a parthenogenetic or a sexual cycle have been studied in brown algae, as has the impact of asexual parthenogenesis on gamete phenotype. For isogamy and weak anisogamy, gametes of both sexes undergo parthenogenesis; however, there is a difference in germination success. For example, in *Scytosiphon lomentaria* culture experiments, more than 50% of the female gametes achieved a greater than 4-cell stage but less than 5% of the male gametes reached this stage.[70] The low survival rate of parthenogenetic offspring suggests that parthenogenesis is a back-up plan for fertilization failures, especially where mating inefficiency exists.[69,71] For example, Japanese *S. lomentaria* sexual populations (composed of two sexes) inhabit calm waters, but parthenogenetic (unisexual female) populations grow in unfavorable and wave-exposed

Please cite this article in press as: Choi et al., Ordovician origin and subsequent diversification of the brown algae, Current Biology (2023), https://doi.org/10.1016/j.cub.2023.12.069

areas.[70,72] This mimics patterns of land plant geographical parthenogenesis where parthenogenetic groups are predominant and outcompete the sexual relatives under unfavorable and marginal conditions.[69,71,73] In general, parthenogenetic lineages of *S. lomentaria* acquire a significantly larger gamete size (i.e., parthenogenetic gametes: ca. 5.0–6.0 μm, sexual gametes: ca. 3.4–4.5 μm in diameter).[70] Moreover, some of the parthenogenetic female populations have independently lost their ability to produce pheromones that attract male gametes,[72] further strengthening the asexual pathway. Thus, gamete evolution under different environmental conditions in the brown algae seems to be in agreement with the theoretical prediction.[64]

In this study, evidence that parthenogenesis might maintain isogamy or might cause a reversion to isogamy comes from both the character correlation analysis and the timeline of reversions. The correlation analysis shows that in the parthenogenetic condition, there is a strong preference for isogamy, but under non-parthenogenetic conditions, oogamy is preferred (Figure 3C). It is evident in the fact that the loss of parthenogenesis can be seen in two independent oogamous lineages, the Dictyotales and the Fucales (Figure 3A).[66] In brown algae, centrioles are inherited from male gametes; thus, if unfertilized gametes undergo parthenogenesis, the female centrosomes must correctly work to assure the mechanics of parthenogenesis.[74] However, due to cytological defects of centrosomes in the eggs, Dictyotalean and Fucalean species cannot correctly divide a pair of chromosomes during parthenogenic mitosis, leading to parthenogenic germlings that are aborted at an early stage.[75,76]

Furthermore, our results show that a reversion from oogamy to aniso- or isogamy occurred independently in three ordinal-level lineages: the Ralfsiales-Tilopteridales, the Scytothamnales-Ascoseirales, and the Ectocarpales (see Figure 3A). These independent reversions occurred during the Cretaceous Period (except the *Akkesiphycus*-case), an interval characterized by the highest sea levels of the Phanerozoic Eon.[77] Rising sea levels and episodic continental flooding expanded shallow marine habitats, facilitating the diversification of macroalgae.[77,78] In marginal new habitats, parthenogenetic lineages have several advantages in reproductive assurance and fast colonization compared with their sexual counterparts.[73] In the case of brown alga *S. lomentaria*, parthenogenetic populations were preferentially located in the wave-exposed high intertidal areas.[72] A schematic model of gamete evolution, combining the geological interpretations and character estimation results, is summarized in Figure 3F.

Gamete evolution theory suggests that anisogamous and oogamous conditions evolved from an unstable isogamous condition.[65] In a developmental sense, it is difficult for an egg to revert back to an iso- or anisogamous gamete because it requires the reformation of microtubular flagellar structures.[79] Therefore, the transition to oogamy has been thought of as an evolutionary dead end where reversions are impossible. However, most oogamous brown algal lineages (except diplontic Fucales) produce biflagellate meiospores regardless of the sex chromosome they carry (i.e., U or V chromosome). These meiospores develop into gametophytes that subsequently produce gametes in a later stage.[80] The presence of flagella on all meiospores suggests that the absence of flagella on oogamous eggs is not caused by the absence of flagellar genes. Furthermore, the kelp *Saccharina angustata* has female gametes that possess "egg flagella" even though this species is phylogenetically nested within the oogamous Laminariales.[81] These egg flagella have an atypical 8 + 2 microtubular structure and are functionally nonmotile. However, egg flagella ensure close contact between the zygote and the oogonial wall and help orient the cell polarity axis,[82] which suggests that egg flagella are not a vestigial structure but a *de novo* functional acquisition. That is, flagellar development on the egg is under genetic regulation and gene expression control. The loci responsible for this life-stage-specific regulation may be encoded in the sex-determining region (SDR) or in a sex chromosome. Interestingly, the related species *Saccharina latissima* has a low expression of male development genes (e.g., flagella-related genes) in the female gametophyte.[83] Expression comparisons between *Saccharina latissima* (a true oogamous species) and *Saccharina angustata* (egg-flagellated species) could help decipher the regulation of the flagellar development in female gametes and its involved loci. Overall, the presence of flagella in all meiospores and in the flagellated egg in *S. angustata* suggests that secondary reversion from oogamy to isogamy in the brown algae is a possible evolutionary scenario. Aside from brown algae, a reversion from oogamy to anisogamy has also been reported once in the Volvocine algae (i.e., the anisogamous *Pleodorina japonica* within the oogamous *Volvox* clade).[84]

Our study of the sexual evolution of brown algae shares some overlap with a previous study[21]; however, our study shows progress in three different aspects: (1) phylogeny, (2) time estimation, and (3) character estimation. Phylogeny is crucial because character changes are mapped onto specific brown algal lineages. Our study, which used plastomes, was the first to recover the close evolutionary relationship of two isogamous classes (Scytothamnales and Ascoseirales), which was not detected in the phylogeny of an earlier study.[21] Regarding time estimation, our study was the first to suggest possible paleo-environmental reasons for gametic reversions. We determined the geological age when the reversals occurred, and then we described paleo-environmental changes that happened during that geological time. Finally, we used character estimation to show that early-diverged brown algae were isogamous. Two previous studies[21,22] concluded that the ancestral brown algae were oogamous. In summary, our new timelines for brown algae combined with a knowledge of past environments shed new light on brown algal diversification and the intertwined evolution of multicellularity and sexual reproduction.

STAR★METHODS

Detailed methods are provided in the online version of this paper and include the following:

- KEY RESOURCES TABLE
- RESOURCE AVAILABILITY
  - Lead contact
  - Materials availability
  - Data and code availability
- EXPERIMENTAL MODEL AND SUBJECT DETAILS
- METHOD DETAILS
  - DNA extraction, whole-genome sequencing and sequence data analysis

- Genome assembly and annotation
- Phylogenetic tree construction and robustness analyses
- Divergence time estimation and clock model testing
- Ancestral character estimation, transition rates, correlation and comparison analyses

- QUANTIFICATION AND STATISTICAL ANALYSIS

SUPPLEMENTAL INFORMATION

Supplemental information can be found online at https://doi.org/10.1016/j.cub.2023.12.069.

ACKNOWLEDGMENTS

The authors thank John A. West at the University of Melbourne, who provided *Dictyotopsis propagulifera* JAW4848. This study was supported by the National Research Foundation of Korea (NRF-2022R1A2B5B03002312, 2022R1A5A1031361, 2019H1A2A1073652-Global Ph.D. Fellowship Program), the Korea Institute of Marine Science and Technology Promotion (KIMST) funded to the Ministry of Oceans and Fisheries (MOF) (grant numbers 20180430, 20210469), and the Cooperative Research Program for Agriculture Science and Technology Development (project no. RS-2023-00231243), Rural Development Administration, Republic of Korea.

AUTHOR CONTRIBUTIONS

S.-W.C., L.G., and H.S.Y. designed the study. S.-W.C., J.W.C., L.G., J.J., G.H.B., H.K., C.G.C., and H.S.Y. acquired field samples and produced the data (DNA extraction, sequencing, and bioinformatics). S.-W.C., L.G., and J.J. analyzed data. S.-W.C., L.G., G.H.B., H.K., S.X., A.H.K., R.A.A., and H.S.Y. interpreted the results. S.-W.C., L.G., H.K., S.X., A.H.K., R.A.A., and H.S.Y. wrote the manuscript. All authors read and approved the final manuscript.

DECLARATION OF INTERESTS

The authors declare no competing interests.

Received: November 6, 2023
Revised: December 8, 2023
Accepted: December 20, 2023
Published: January 22, 2024

REFERENCES

1. Guiry, M.D., Moestrup, Ø., and Andersen, R.A. (2023). Validation of the phylum name Heterokontophyta. Not. Algarum *297*, 1–5.
2. Yoon, H.S., Hackett, J.D., Ciniglia, C., Pinto, G., and Bhattacharya, D. (2004). A molecular timeline for the origin of photosynthetic eukaryotes. Mol. Biol. Evol. *21*, 809–818.
3. Guiry, M.D., and Guiry, G. AlgaeBase. https://www.algaebase.org/.
4. Graham, L.E., Graham, J.M., and Wilcox, L.W. (2009). Algae, 2nd Edition (Benjamin Cummings), p. 301.
5. Cock, J.M., Godfroy, O., Macaisne, N., Peters, A.F., and Coelho, S.M. (2014). Evolution and regulation of complex life cycles: a brown algal perspective. Curr. Opin. Plant Biol. *17*, 1–6.
6. Knoll, A.H. (2011). The multiple origins of complex multicellularity. Annu. Rev. Earth Planet. Sci. *39*, 217–239.
7. Terauchi, M., Nagasato, C., and Motomura, T. (2015). Plasmodesmata of brown algae. J. Plant Res. *128*, 7–15.
8. Luthringer, R., Cormier, A., Ahmed, S., Peters, A.F., Cock, J.M., and Coelho, S.M. (2014). Sexual dimorphism in the brown algae. Perspect. Phycol. *1*, 11–25.
9. Kawai, H., Maeba, S., Sasaki, H., Okuda, K., and Henry, E.C. (2003). *Schizocladia ischiensis*: A new filamentous marine chromophyte belonging to a new class, Schizociadiophyceae. Protist *154*, 211–228.
10. Charrier, B., Le Bail, A., and de Reviers, B. (2012). Plant Proteus: brown algal morphological plasticity and underlying developmental mechanisms. Trends Plant Sci. *17*, 468–477.
11. Darwin, C. (1871). The Descent of Man, and Selection in Relation to Sex (John Murray).
12. Smith, J.M. (1971). The origin and maintenance of sex. In Group Selection (Routledge), pp. 163–175.
13. Parker, G.A., Baker, R.R., and Smith, V.G. (1972). The origin and evolution of gamete dimorphism and the male-female phenomenon. J. Theor. Biol. *36*, 529–553.
14. Knowlton, N. (1974). A note on the evolution of gamete dimorphism. J. Theor. Biol. *46*, 283–285.
15. Randerson, J.P., and Hurst, L.D. (2001). A comparative test of a theory for the evolution of anisogamy. Proc. Biol. Sci. *268*, 879–884.
16. Hanschen, E.R., Herron, M.D., Wiens, J.J., Nozaki, H., and Michod, R.E. (2018). Multicellularity drives the evolution of sexual traits. Am. Nat. *192*, E93–E105.
17. Lehtonen, J., and Parker, G.A. (2014). Gamete competition, gamete limitation, and the evolution of the two sexes. Mol. Hum. Reprod. *20*, 1161–1168.
18. Bateman, A.J. (1948). Intra-sexual selection in *Drosophila*. Heredity *2*, 349–368.
19. Lehtonen, J., Parker, G.A., and Schärer, L. (2016). Why anisogamy drives ancestral sex roles. Evolution *70*, 1129–1135.
20. Maier, I. (1995). Brown algal pheromones. Prog. Phycol. Res. *11*, 51–102.
21. Heesch, S., Serrano-Serrano, M., Barrera-Redondo, J., Luthringer, R., Peters, A.F., Destombe, C., Cock, J.M., Valero, M., Roze, D., Salamin, N., and Coelho, S.M. (2021). Evolution of life cycles and reproductive traits: insights from the brown algae. J. Evol. Biol. *34*, 992–1009.
22. Silberfeld, T., Leigh, J.W., Verbruggen, H., Cruaud, C., de Reviers, B., and Rousseau, F. (2010). A multi-locus time-calibrated phylogeny of the brown algae (Heterokonta, Ochrophyta, Phaeophyceae): investigating the evolutionary nature of the "brown algal crown radiation". Mol. Phylogenet. Evol. *56*, 659–674.
23. Cho, G.Y., Lee, S.H., and Boo, S.M. (2004). A new brown algal order, Ishigeales (Phaeophyceae), established on the basis of plastid protein-coding *rbcL*, *psaA*, and *psbA* region comparisons. J. Phycol. *40*, 921–936.
24. Kawai, H., Hanyuda, T., Draisma, S.G., Wilce, R.T., and Andersen, R.A. (2015). Molecular phylogeny of two unusual brown algae, *Phaeostrophion irregulare* and *Platysiphon glacialis*, proposal of the Stschapoviales ord. nov. and Platysiphonaceae fam. nov., and a re-examination of divergence times for brown algal orders. J. Phycol. *51*, 918–928.
25. Parker, B.C., and Dawson, E.Y. (1965). Non-calcareous marine algae from California Miocene deposits. Nova Hedwigia *10*, 273–295.
26. Rajanikanth, A. (1989). A fossil marine brown alga from the Gangapur formation, Pranhita–Godavari graben. Curr. Sci. *58*, 78–80.
27. Abe, K., and Jordan, R.W. (2021). Re-examination of *Archaeomonas mirabilis* from the Late Cretaceous reveals its true identity as the oldest known fossil Parmales (Bolidophyceae). Phycologia *60*, 362–367.
28. Harwood, D.M., Nikolaev, V.A., and Winter, D.M. (2007). Cretaceous records of diatom evolution, radiation, and expansion. Paleontol. Soc. Pap. *13*, 33–59.
29. Behrenfeld, M.J., Halsey, K.H., Boss, E., Karp-Boss, L., Milligan, A.J., and Peers, G. (2021). Thoughts on the evolution and ecological niche of diatoms. Ecol. Monogr. *91*, e01457.
30. Siver, P.A., and Velez, M.I. (2023). The oldest raphe-bearing diatoms: evidence from the Upper Cretaceous of western and northern Canada. Cretac Res. *144*, 105456.

31. Zhang, W., Yang, H., Xia, X., Xie, L., and Xie, G. (2016). Triassic chrysophyte cyst fossils discovered in the Ordos Basin, China. Geology *44*, 1031–1034.
32. Siver, P.A. (2022). The downsizing of gigantic scales and large cells in the genus Mallomonas (Synurales, Chrysophyceae). Sci, Rep. *12*, 4896.
33. Tao, Q., Tamura, K., U Battistuzzi, F., and Kumar, S. (2019). A machine learning method for detecting autocorrelation of evolutionary rates in large phylogenies. Mol. Biol. Evol. *36*, 811–824.
34. Mooers, A.Ø., and Schluter, D. (1999). Reconstructing ancestor states with maximum likelihood: support for one-and two-rate models. Syst. Biol. *48*, 623–633.
35. Moe, R.L., and Henry, E.C. (1982). Reproduction and early development of *Ascoseira mirabilis* Skottsberg (Phaeophyta), with notes on Ascoseirales Petrov. Phycologia *21*, 55–66.
36. Gilks, R., and Richardson, S. (1996). Spiegelhalter. Markov Chain Monte Carlo in Practice (Chapman and Hall/CRC).
37. Brown, J.W., and Sorhannus, U. (2010). A molecular genetic timescale for the diversification of autotrophic stramenopiles (Ochrophyta): substantive underestimation of putative fossil ages. PLoS One *5*, e12759.
38. Medlin, L.K., Kooistra, W.H.C.F., Potter, D., Saunders, G.W., and Andersen, R.A. (1997). Phylogenetic relationships of the 'golden algae' (haptophytes, heterokont chromophytes) and their plastids. In Origins of Algae and their Plastids (Springer), pp. 187–219.
39. Bromham, L., Duchêne, S., Hua, X., Ritchie, A.M., Duchêne, D.A., and Ho, S.Y.W. (2018). Bayesian molecular dating: opening up the black box. Biol. Rev. Camb. Philos. Soc. *93*, 1165–1191.
40. Parfrey, L.W., Lahr, D.J., Knoll, A.H., and Katz, L.A. (2011). Estimating the timing of early eukaryotic diversification with multigene molecular clocks. Proc. Natl. Acad. Sci. USA *108*, 13624–13629.
41. Strassert, J.F.H., Irisarri, I., Williams, T.A., and Burki, F. (2021). A molecular timescale for eukaryote evolution with implications for the origin of red algal-derived plastids. Nat. Commun. *12*, 1879.
42. Holland, S.M. (2016). The non-uniformity of fossil preservation. Philos. Trans. R. Soc. Lond. B Biol. Sci. *371*, 20150130.
43. Lucas, W.J., Ham, B.-K., and Kim, J.-Y. (2009). Plasmodesmata–bridging the gap between neighboring plant cells. Trends Cell Biol. *19*, 495–503.
44. Boraas, M.E., Seale, D.B., and Boxhorn, J.E. (1998). Phagotrophy by a flagellate selects for colonial prey: a possible origin of multicellularity. Evol. Ecol. *12*, 153–164.
45. Lurling, M., and Beekman, W. (2006). Palmelloids formation in Chlamydomonas reinhardtii: defence against rotifer predators? Ann. Limnol. - Int. J. Lim. *42*, 65–72.
46. Knoll, A.H., and Lahr, D. (2016). Fossils, feeding, and the evolution of complex multicellularity. In Multicellularity, Origins and Evolution, K.J. Niklas, and S.A. Newman, eds. (The MIT Press), pp. 1–16.
47. Bykova, N., LoDuca, S.T., Ye, Q., Marusin, V., Grazhdankin, D., and Xiao, S. (2020). Seaweeds through time: morphological and ecological analysis of Proterozoic and Early Paleozoic benthic macroalgae. Precambrian Res. *350*, 105875.
48. LoDuca, S.T., Bykova, N., Wu, M., Xiao, S., and Zhao, Y. (2017). Seaweed morphology and ecology during the great animal diversification events of the early Paleozoic: a tale of two floras. Geobiology *15*, 588–616.
49. Knoll, A.H., and Carroll, S.B. (1999). Early animal evolution: emerging views from comparative biology and geology. Science *284*, 2129–2137.
50. Lindskog, A., Young, S.A., Bowman, C.N., Kozik, N.P., Newby, S.M., Eriksson, M.E., Pettersson, J., Molin, E., and Owens, J.D. (2023). Oxygenation of the Baltoscandian shelf linked to Ordovician biodiversification. Nat. Geosci. *16*, 1047–1053.
51. Dahl, T.W., Hammarlund, E.U., Anbar, A.D., Bond, D.P., Gill, B.C., Gordon, G.W., Knoll, A.H., Nielsen, A.T., Schovsbo, N.H., and Canfield, D.E. (2010). Devonian rise in atmospheric oxygen correlated to the radiations of terrestrial plants and large predatory fish. Proc. Natl. Acad. Sci. USA *107*, 17911–17915.
52. Wallace, M.W., Hood, A., Shuster, A., Greig, A., Planavsky, N.J., and Reed, C.P. (2017). Oxygenation history of the Neoproterozoic to Early Phanerozoic and the rise of land plants. Earth Planet. Sci. Lett. *466*, 12–19.
53. Hammarlund, E.U., Flashman, E., Mohlin, S., and Licausi, F. (2020). Oxygen-sensing mechanisms across eukaryotic kingdoms and their roles in complex multicellularity. Science *370*, eaba3512.
54. Coelho, S.M., Brownlee, C., and Bothwell, J.H. (2008). Feedback control of reactive oxygen and Ca2+ signalling during brown algal embryogenesis. Plant Signal. Behav. *3*, 570–572.
55. Coelho, S.M., Taylor, A.R., Ryan, K.P., Sousa-Pinto, I., Brown, M.T., and Brownlee, C. (2002). Spatiotemporal patterning of reactive oxygen production and Ca2+ wave propagation in *Fucus* rhizoid cells. Plant Cell *14*, 2369–2381.
56. Knoll, A.H., Summons, R.E., Waldbauer, J.R., and Zumberge, J.E. (2007). The geological succession of primary producers in the oceans. In Evolution of Primary Producers in the Sea (Elsevier), pp. 133–163.
57. Bulmer, M.G., and Parker, G.A. (2002). The evolution of anisogamy: a game-theoretic approach. Proc. Biol. Sci. *269*, 2381–2388.
58. Schettino, A., and Turco, E. (2009). Breakup of Pangaea and plate kinematics of the central Atlantic and Atlas regions. Geophys. J. Int. *178*, 1078–1097.
59. Katz, M.E., Finkel, Z.V., Grzebyk, D., Knoll, A.H., and Falkowski, P.G. (2004). Evolutionary trajectories and biogeochemical impacts of marine eukaryotic phytoplankton. Annu. Rev. Ecol. Evol. Syst. *35*, 523–556.
60. Kirk, D.L. (2005). A twelve-step program for evolving multicellularity and a division of labor. BioEssays *27*, 299–310.
61. Nishiyama, T., Sakayama, H., De Vries, J., Buschmann, H., Saint-Marcoux, D., Ullrich, K.K., Haas, F.B., Vanderstraeten, L., Becker, D., and Lang, D. (2018). The Chara genome: secondary complexity and implications for plant terrestrialization. Cell *174*, 448–464.e24.
62. Cheng, S., Xian, W., Fu, Y., Marin, B., Keller, J., Wu, T., Sun, W., Li, X., Xu, Y., Zhang, Y., et al. (2019). Genomes of subaerial Zygnematophyceae provide insights into land plant evolution. Cell *179*, 1057–1067.e14.
63. Ispolatov, I., Ackermann, M., and Doebeli, M. (2012). Division of labour and the evolution of multicellularity. Proc. Biol. Sci. *279*, 1768–1776.
64. Lehtonen, J., Horinouchi, Y., Togashi, T., and Parker, G.A. (2021). Evolution of anisogamy in organisms with parthenogenetic gametes. Am. Nat. *198*, 360–378.
65. Togashi, T., Bartelt, J.L., Yoshimura, J., Tainaka, K.-I., and Cox, P.A. (2012). Evolutionary trajectories explain the diversified evolution of isogamy and anisogamy in marine green algae. Proc. Natl. Acad. Sci. USA *109*, 13692–13697.
66. Nagasato, C. (2005). Behavior and function of paternally inherited centrioles in brown algal zygotes. J. Plant Res. *118*, 361–369.
67. Knoll, A.H., and Follows, M.J. (2016). A bottom-up perspective on ecosystem change in Mesozoic oceans. Proc. Biol. Sci. *283*, 20161755.
68. Pearson, G.A., and Brawley, S.H. (1996). Reproductive ecology, of *Fucus distichus* (Phaeophyceae): an intertidal alga with successful external fertilization. Mar. Ecol. Prog. Ser. *143*, 211–223.
69. Hörandl, E. (2006). The complex causality of geographical parthenogenesis. New Phytol. *171*, 525–538.
70. Hoshino, M., Okino, T., and Kogame, K. (2019). Parthenogenetic female populations in the brown alga *Scytosiphon lomentaria* (Scytosiphonaceae, Ectocarpales): decay of a sexual trait and acquisition of asexual traits. J. Phycol. *55*, 204–213.
71. Bierzychudek, P. (1985). Patterns in plant parthenogenesis. Experientia *41*, 1255–1264.
72. Hoshino, M., Hiruta, S.F., Croce, M.E., Kamiya, M., Jomori, T., Wakimoto, T., and Kogame, K. (2021). Geographical parthenogenesis in the brown alga *Scytosiphon lomentaria* (Scytosiphonaceae): sexuals in warm waters and parthenogens in cold waters. Mol. Ecol. *30*, 5814–5830.

73. Kearney, M. (2005). Hybridization, glaciation and geographical parthenogenesis. Trends Ecol. Evol. *20*, 495–502.
74. Motomura, T., Nagasato, C., and Kimura, K. (2010). Cytoplasmic inheritance of organelles in brown algae. J. Plant Res. *123*, 185–192.
75. Nagasato, C., Motomura, T., and Ichimura, T. (2000). Parthenogenesis and abnormal mitosis in unfertilized eggs of *Fucus distichus* (Fucales, Phaeophyceae). Phycologia *39*, 163–166.
76. Williams, J.L. (1904). Studies in the Dictyotaceae. II. The cytology of the gametophyte generation. Ann. Bot. *18*, 183–204.
77. Miller, K.G., Kominz, M.A., Browning, J.V., Wright, J.D., Mountain, G.S., Katz, M.E., Sugarman, P.J., Cramer, B.S., Christie-Blick, N., and Pekar, S.F. (2005). The Phanerozoic record of global sea-level change. Science *310*, 1293–1298.
78. Falkowski, P.G., Katz, M.E., Knoll, A.H., Quigg, A., Raven, J.A., Schofield, O., and Taylor, F.J. (2004). The evolution of modern eukaryotic phytoplankton. Science *305*, 354–360.
79. Hackenberg, D., and Twell, D. (2019). The evolution and patterning of male gametophyte development. Curr. Top. Dev. Biol. *131*, 257–298.
80. Kawai, H., and Henry, E. (2017). Phaeophyta. In Handbook of the Protists (Springer).
81. Motomura, T., and Sakai, Y. (1988). The occurrence of flagellated eggs in *Laminaria angustata* (Phaeophyta, Laminariales). J. Phycol. *24*, 282–285.
82. Klochkova, T.A., Motomura, T., Nagasato, C., Klimova, A.V., and Kim, G.H. (2019). The role of egg flagella in the settlement and development of zygotes in two *Saccharina* species. Phycologia *58*, 145–153.
83. Pearson, G.A., Martins, N., Madeira, P., Serrão, E.A., and Bartsch, I. (2019). Sex-dependent and-independent transcriptional changes during haploid phase gametogenesis in the sugar kelp *Saccharina latissima*. PLoS One *14*, e0219723.
84. Umen, J., and Coelho, S. (2019). Algal sex determination and the evolution of anisogamy. Annu. Rev. Microbiol. *73*, 267–291.
85. Paradis, E., Claude, J., and Strimmer, K. (2004). APE: analyses of Phylogenetics and Evolution in R language. Bioinformatics *20*, 289–290.
86. Laslett, D., and Canback, B. (2004). ARAGORN, a program to detect tRNA genes and tmRNA genes in nucleotide sequences. Nucleic Acids Res. *32*, 11–16.
87. Zhang, C., Rabiee, M., Sayyari, E., and Mirarab, S. (2018). ASTRAL-III: polynomial time species tree reconstruction from partially resolved gene trees. BMC Bioinformatics *19*, 153.
88. Pagel, M., Meade, A., and Barker, D. (2004). Bayesian estimation of ancestral character states on phylogenies. Syst. Biol. *53*, 673–684.
89. Langmead, B., and Salzberg, S.L. (2012). Fast gapped-read alignment with Bowtie 2. Nat. Meth. *9*, 357–359.
90. Kearse, M., Moir, R., Wilson, A., Stones-Havas, S., Cheung, M., Sturrock, S., Buxton, S., Cooper, A., Markowitz, S., Duran, C., et al. (2012). Geneious Basic: an integrated and extendable desktop software platform for the organization and analysis of sequence data. Bioinformatics *28*, 1647–1649.
91. Tillich, M., Lehwark, P., Pellizzer, T., Ulbricht-Jones, E.S., Fischer, A., Bock, R., and Greiner, S. (2017). GeSeq – versatile and accurate annotation of organelle genomes. Nucleic Acids Res. *45*, W6–W11.
92. Minh, B.Q., Schmidt, H.A., Chernomor, O., Schrempf, D., Woodhams, M.D., von Haeseler, A., and Lanfear, R. (2020). IQ-TREE 2: new models and efficient methods for phylogenetic inference in the genomic era. Mol. Biol. Evol. *37*, 1530–1534.
93. Katoh, K., and Standley, D.M. (2013). MAFFT multiple sequence alignment software version 7: improvements in performance and usability. Mol. Biol. Evol. *30*, 772–780.
94. Rannala, B., and Yang, Z. (2007). Inferring speciation times under an episodic molecular clock. Syst. Biol. *56*, 453–466.
95. Kalyaanamoorthy, S., Minh, B.Q., Wong, T.K.F., von Haeseler, A., and Jermiin, L.S. (2017). ModelFinder: fast model selection for accurate phylogenetic estimates. Nat. Meth. *14*, 587–589.
96. Dierckxsens, N., Mardulyn, P., and Smits, G. (2017). NOVOPlasty: de novo assembly of organelle genomes from whole genome data. Nucleic Acids Res. *45*, e18.
97. Suyama, M., Torrents, D., and Bork, P. (2006). PAL2NAL: robust conversion of protein sequence alignments into the corresponding codon alignments. Nucleic Acids Res. *34*, W609–W612.
98. Brown, J.W., Walker, J.F., and Smith, S.A. (2017). Phyx: phylogenetic tools for unix. Bioinformatics *33*, 1886–1888.
99. Li, H., Handsaker, B., Wysoker, A., Fennell, T., Ruan, J., Homer, N., Marth, G., Abecasis, G., and Durbin, R.; 1000 Genome Project Data Processing Subgroup (2009). The Sequence Alignment/Map format and SAMtools. Bioinformatics *25*, 2078–2079.
100. Bankevich, A., Nurk, S., Antipov, D., Gurevich, A.A., Dvorkin, M., Kulikov, A.S., Lesin, V.M., Nikolenko, S.I., Pham, S., Prjibelski, A.D., et al. (2012). SPAdes: a new genome assembly algorithm and its applications to single-cell sequencing. J. Comput. Biol. *19*, 455–477.
101. Rambaut, A., Drummond, A.J., Xie, D., Baele, G., and Suchard, M.A. (2018). Posterior summarization in Bayesian phylogenetics using Tracer 1.7. Syst. Biol. *67*, 901–904.
102. Guillard, R.R.L., and Hargraves, P.E. (1993). *Stichochrysis immobilis* is a diatom, not a chrysophyte. Phycologia *32*, 234–236.
103. Choi, J.W., Graf, L., Peters, A.F., Cock, J.M., Nishitsuji, K., Arimoto, A., Shoguchi, E., Nagasato, C., Choi, C.G., and Yoon, H.S. (2020). Organelle inheritance and genome architecture variation in isogamous brown algae. Sci. Rep. *10*, 2048.
104. Song, H.J., Lee, J., Graf, L., Rho, M., Qiu, H., Bhattacharya, D., and Yoon, H.S. (2016). A novice's guide to analyzing NGS-derived organelle and metagenome data. Algae *31*, 137–154.
105. Altschul, S.F., Madden, T.L., Schäffer, A.A., Zhang, J.H., Zhang, Z., Miller, W., and Lipman, D.J. (1997). Gapped BLAST and PSI-BLAST: a new generation of protein database search programs. Nucleic Acids Res. *25*, 3389–3402.
106. Chernomor, O., von Haeseler, A., and Minh, B.Q. (2016). Terrace aware data structure for phylogenomic inference from supermatrices. Syst. Biol. *65*, 997–1008.
107. Hoang, D.T., Chernomor, O., von Haeseler, A., Minh, B.Q., and Vinh, L.S. (2018). UFBoot2: improving the ultrafast bootstrap approximation. Mol. Biol. Evol. *35*, 518–522.
108. Kishino, H., Miyata, T., and Hasegawa, M. (1990). Maximum likelihood inference of protein phylogeny and the origin of chloroplasts. J. Mol. Evol. *31*, 151–160.
109. Kishino, H., and Hasegawa, M. (1989). Evaluation of the maximum likelihood estimate of the evolutionary tree topologies from DNA sequence data, and the branching order in Hominoidea. J. Mol. Evol. *29*, 170–179.
110. Shimodaira, H., and Hasegawa, M. (1999). Multiple comparisons of log-likelihoods with applications to phylogenetic inference. Mol. Biol. Evol. *16*, 1114–1116.
111. Strimmer, K., and Rambaut, A. (2002). Inferring confidence sets of possibly misspecified gene trees. Proc. Biol. Sci. *269*, 137–142.
112. Shimodaira, H. (2002). An approximately unbiased test of phylogenetic tree selection. Syst. Biol. *51*, 492–508.
113. Naser-Khdour, S., Minh, B.Q., Zhang, W.Q., Stone, E.A., and Lanfear, R. (2019). The prevalence and impact of model violations in phylogenetic analysis. Genome Biol. Evol. *11*, 3341–3352.
114. Felsenstein, J. (2004). Inferring Phylogenies (Sinauer Associates).
115. Sayyari, E., and Mirarab, S. (2016). Fast coalescent-based computation of local branch support from quartet frequencies. Mol. Biol. Evol. *33*, 1654–1668.
116. dos Reis, M.d., and Yang, Z. (2011). Approximate likelihood calculation on a phylogeny for Bayesian estimation of divergence times. Mol. Biol. Evol. *28*, 2161–2172.

117. Smith, S.A., Brown, J.W., and Walker, J.F. (2018). So many genes, so little time: a practical approach to divergence-time estimation in the genomic era. PLoS One *13*, e0197433.

118. Ho, S.Y., and Phillips, M.J. (2009). Accounting for calibration uncertainty in phylogenetic estimation of evolutionary divergence times. Syst. Biol. *58*, 367–380.

119. Steiner, M. (1994). Die Neoproterozoischen Megaalgen Südchinas. Berliner Geowissenschaftliche Abhandlungen (E) *15*, 1–146.

120. Xiao, S., Knoll, A.H., and Yuan, X. (1998). Morphological reconstruction of *Miaohephyton bifurcatum*, a possible brown alga from the Neoproterozoic Doushantuo Formation, South China. J. Paleontol. *72*, 1072–1086.

121. Butterfield, N.J. (2015). Proterozoic photosynthesis–a critical review. Palaeontology *58*, 953–972.

122. R Core Team (2013). R: A Language and Environment for Statistical Computing (R Foundation for Statistical Computing).

123. Xie, W., Lewis, P.O., Fan, Y., Kuo, L., and Chen, M.-H. (2011). Improving marginal likelihood estimation for Bayesian phylogenetic model selection. Syst. Biol. *60*, 150–160.

124. Vranken, S., Robuchon, M., Dekeyzer, S., Bárbara, I., Bartsch, I., Blanfuné, A., Boudouresque, C.-F., Decock, W., Destombe, C., and de Reviers, B. (2022). AlgaeTraits: a trait database for (European) seaweeds. Earth Syst. Sci. Data Discuss. *15*, 2711–2754.

Please cite this article in press as: Choi et al., Ordovician origin and subsequent diversification of the brown algae, Current Biology (2023), https://doi.org/10.1016/j.cub.2023.12.069

STAR★METHODS

KEY RESOURCES TABLE

REAGENT or RESOURCE	SOURCE	IDENTIFIER
Deposited data		
Plastid genome maps	NCBI GenBank	GenBank: ON527003, ON552953-ON552976, OR757060-OR757061
Software or algorithms		
APE	Paradis et al.[85]	https://cran.r-project.org/web/packages/ape/index.html
ARAGORN v1.2.38	Laslett and Canback[86]	http://www.ansikte.se/ARAGORN/
ASTRAL-III	Zhang et al.[87]	https://github.com/smirarab/ASTRAL
BayesTraits v3.0.5	Pagel et al.[88]	http://www.evolution.reading.ac.uk/BayesTraitsV3.0.5/
Bowtie 2 v2.3.5.1	Langmead and Salzberg[89]	https://github.com/BenLangmead/bowtie2
CorrTest	Tao et al.[33]	https://github.com/cathyqqtao/CorrTest
Geneious Prime 2019.0.3	Kearse et al.[90]	https://www.geneious.com/
GeSeq v2.03	Tillich et al.[91]	https://chlorobox.mpimp-golm.mpg.de/geseq.html
IQ-TREE 2	Minh et al.[92]	http://www.iqtree.org/
MAFFT v7	Katoh and Standley[93]	https://mafft.cbrc.jp/alignment/software/
MCMCTree	Rannala and Yang[94]	http://abacus.gene.ucl.ac.uk/software/paml.html
ModelFinder	Kalyaanamoorthy et al.[95]	http://www.iqtree.org/ModelFinder/
NOVOPlasty v3.7	Dierckxsens et al.[96]	https://github.com/ndierckx/NOVOPlasty
PAL2NAL	Suyama et al.[97]	https://www.bork.embl.de/pal2nal/
Phyx	Brown et al.[98]	https://github.com/FePhyFoFum/phyx
SAMtools v1.5	Li et al.[99]	https://github.com/samtools/samtools
SPAdes v3.11.1	Bankevich et al.[100]	https://github.com/ablab/spades
Tracer v1.7.2	Rambaut et al.[101]	https://beast.community/tracer

RESOURCE AVAILABILITY

Lead contact

Further requests for information or resources should be directed to the lead contact, Hwan Su Yoon (hsyoon2011@skku.edu).

Materials availability

In this study, no new unique reagents were generated.

Data and code availability

- The plastid genome data that are produced in this study were publicly deposited under the accession numbers ON527003, ON552953-ON552976 and OR757060-OR757061 in the NCBI nucleotide database (see Data S1A).
- This paper does not report any original code.
- Additional information regarding this study is available upon request from the lead contact.

EXPERIMENTAL MODEL AND SUBJECT DETAILS

Seven brown algal strains were provided by the Kobe University Macroalgal Culture Collection (KU-MACC), one strain (*Ascoseira mirabilis*) by Provasoli-Guillard National Center for Marine Algae and Microbiota (NCMA) and *Dictyotopsis propagulifera* JAW4848 was obtained from Dr. J.A. West, University of Melbourne (Data S1B). Strains were grown in enriched seawater L1 medium[102] and maintained in culture chambers at 15°C under a 12:12 hr light:dark cycle. Eleven brown algal species were collected from natural habitats by S.-W.C., C.G.C., L.G., and H.S.Y. (Data S1B). Collected thalli were washed in autoclaved seawater, and paper towels were used to remove potential epiphytes; thalli were then air-dried in silica gel.

Please cite this article in press as: Choi et al., Ordovician origin and subsequent diversification of the brown algae, Current Biology (2023), https://doi.org/10.1016/j.cub.2023.12.069

METHOD DETAILS

DNA extraction, whole-genome sequencing and sequence data analysis

Genomic DNA was extracted from approximately 1.5 mg of dried material that was frozen in liquid nitrogen and pulverized using an Automill TK-AM5 frozen crusher crusher (Tokken Inc., Kashiwa, Japan). For all species, DNA was extracted using the DNeasy Plant Mini Kit (Qiagen, Hilden, Germany). Whole-genome sequencing was performed either on an Ion Torrent PGM platform (Life Technologies, San Francisco, CA, USA), an Illumina NovaSeq 6000 platform or a MiSeq platform (Illumina, San Diego, CA, USA). For the Ion Torrent PGM platform, Ion Xpress Plus Fragment Library Kit (Thermo Fisher Scientific, San Francisco, CA, USA) was used to prepare 400 bp-sized libraries. An Ion PGM Hi-Q OT2 Kit-400 and an Ion PGM Hi-Q Sequencing Kit (Thermo Fisher Scientific) were used for genome sequencing. A 550 bp-sized library was prepared for the Illumina sequencing platform, which used a TruSeq DNA Nano protocol. Illumina library constructions and sequencing were conducted at DNA-Link Co. (Seoul, Korea). DNA sequence data for ten brown algal species (*Analipus japonicus*, *Cymathaere triplicata*, *Dictyoneurum californicum*, *Hedophyllum nigripes*, *Lessonia variegata*, *Nereocystis luetkeana*, *Padina crassa*, *Pelagophycus porra*, *Pleurophycus gardneri*, *Scytosiphon lomentaria*), four chrysophytes (*Chromulina nebulosa*, *Dinobryon nebulosa*, *Epipyxis* sp., *Hydrurus foetidus*) and one pinguiophyte (*Pinguiococcus pyrenoidosus*) were retrieved from the NCBI Sequence Read Archive (Data S1B).

Genome assembly and annotation

Details for the organelle genome assembly pipeline using PGM reads were described in Choi et al.[103] and Song et al.[104] Ion Torrent PGM reads were assembled with SPAdes v3.11.1[100] and the CLC Genomics Workbench *de novo* assembly function (v5.5.1, CLC bio, Aarhus, Denmark). Assembled contigs were screened for homology with the protein sequences of *Ectocarpus siliculosus* plastomes (NC_013498.1) using tblastn v2.2.31.[105] The sorted contigs were finally circularized using the Geneious Prime 2019.0.3.[90] Illumina reads were assembled with NOVOPlasty v3.7,[96] using the *rbc*L sequence as a seed for the assembly of the plastomes. Assembled genomes were polished by aligning sequencing reads using Bowtie 2 v2.3.5.1[89] and processed with SAMtools v1.5.[99] The polished assemblies were annotated with GeSeq v2.03[91] and manually curated using Geneious Prime 2019.0.3, blastn and blastp v2.2.31[105] to find unannotated small CDSs or adjust coding frames. tRNAs and tmRNAs were annotated with ARAGORN v1.2.38.[86]

Phylogenetic tree construction and robustness analyses

For construction of the brown algal maximum-likelihood (ML) phylogeny, we used 138 plastomes including 118 stramenopiles and 20 outgroup taxa consisting of red algae, cryptophytes, haptophytes. Among the 138 plastomes data, 35 plastomes were newly sequenced or assembled (Data S1B). A total of 141 CDS amino acid sequences, which were conserved in the brown plastomes, were selected to infer a phylogenetic relationship for the brown algae. The sequences were aligned with MAFFT v7 (–maxiterate 1000 option)[93] and concatenated with Phyx.[98] For further phylogenetic analysis with a nucleotide dataset, a codon alignment was constructed using nucleotide and amino acid alignments with PAL2NAL.[97] Alignments were partitioned based on genes. The protein substitution model for phylogenetic analyses with the amino acid alignment was selected using ModelFinder.[95] Maximum-likelihood phylogenetic trees using the sequences were constructed with IQ-TREE 2,[92] allowing each partition to have its own branch length.[106] Statistical support for each branch of the trees was tested via 1,000 replicates of ultrafast bootstrap (UFBoot).[107]

Alternative scenarios for alternative phylogenetic relationship and gamete evolution were tested with alternative tree topology tests. Tree topology tests with constrained alternative topologies were conducted with bootstrap proportion tests using resampling estimated log-likelihoods (RELL),[108] a weighted Kishino-Hasegawa (KH) test,[109] a weighted Shimodaira-Hasegawa (SH) test,[110] an expected likelihood weight (ELW) test[111] and an approximately unbiased (AU) test.[112] RELL was set to 10,000 for the tests.

We conducted tests of symmetry with IQ-TREE 2, which tested whether each marker violated the assumptions of phylogenetic methods.[113] According to the extent to which each gene violates the assumptions in phylogenetic models such as homogeneity (constant substitution rates) and stationary (constant frequencies of nucleotides or amino acids),[114] each gene was assigned with symmetry test *p*-value. Gene sequences were accumulated with a decreasing order of symmetry test *p*-values (that is, genes that were more loyal to the phylogenetic assumptions were first combined) to reconstruct phylogenetic trees with the same options of IQ-TREE 2.

Nucleotide gene trees made with IQ-TREE 2 were used as inputs in coalescent-based species tree estimation with ASTRAL-III.[87] The branches showing less than 10% bootstrap support were collapsed in gene trees before analysis. The support of the coalescent trees was estimated by local posterior probability.[115]

Divergence time estimation and clock model testing

The dataset was over-represented by the Laminariales (40 spp.); therefore, we excluded 27 plastomes to obtain an unbiased taxon usage for our time estimation. We kept only a single species in each genus and excluded other redundant species in the brown algae. We also excluded outgroup taxa and focused on stramenopiles. A total of 77 plastid genes that are shared among all heterokontophyte species were selected for time estimation. Divergence time estimations were performed with MCMCtree (PAML

Please cite this article in press as: Choi et al., Ordovician origin and subsequent diversification of the brown algae, Current Biology (2023), https://doi.org/10.1016/j.cub.2023.12.069

packagev4.9j).[94] The Bayesian calculation efficiency of MCMCtree was increased with the approximate likelihood method.[116] We tested variations of the time estimation result with respect to different selections of priors and data selection. (i) In terms of protein substitution model, we specified the cpREV or WAG model for protein sequences. (ii) Regarding choice of relaxed clock model, we tested uncorrelated and autocorrelated clock models. (iii) Whether selection of different gene data lead to different estimation results was tested. Selection of the most clock-like genes (20, 40, 60 genes) were performed with SortaDate[117] and the result with selected genes were compared to total-gene time tree (77 genes). (iv) Regarding fossil calibration scheme, we adopted two different prior strategies. We compared soft bound calibration, which assigns 2.5% of possibility to outside of the maximum or minimum age, and hard bound calibration, which posits near-zero (1e-300%) possibility to predate maximum or postdate minimum.

Eight fossil priors were used as constraints for time estimation (three brown algae, two diatoms, one parmales, two chrysophytes, see Table 2). Two Cenozoic brown algal fossils from the Monterey Formation, California, show features of the Sargassaceae (*Paleocystophora* and *Paleohalidrys*) and the *Pelagophycus-Nereocystis* clade (*Julescraneia*), and these were applied as recent brown algal calibration points.[25] An Early Cretaceous fossil (100 Ma) from Gangapur formation, India, resembling extant calcifying species *Padina*, was used as constraint for Dictyotales.[26] Two credible fossils for the diatoms (Helmet-shaped diatom epivalve from the Lower Cretaceous Jasong Synthem, South Korea[28] and raphe-bearing *Eunotia*-like fossil[30]) were used as constraints for crown diatom and stem raphid diatom nodes. It has been argued that the origin of crown group diatoms would not predate the Triassic Period due to the lack of fossils and biomarkers specific to diatoms (highly branched isoprenoids, HBI) prior to the mid-Cretaceous.[29] Therefore, we set the maximum age for diatoms as 240 Ma, but assigned the soft bound as mentioned above, to take the possibility of pre-Triassic existence of diatoms into consideration. The oldest parmalean fossil that was recently discovered (*Tetraparma* aff. *mirabilis* from Campbell Plateau, South Pacific[27]) was assigned to the crown Parmales node. The two chrysophytes fossils (cyst fossils from the Ordos Basin, 228 Ma[31] and *Mallomonas* fossil from the 83 Ma Cretaceous Wombat locality[32]) were assigned to the crown Chrysophyceae and Synurales nodes, respectively (Table 2). The maximum constraints for two fossils were assigned with adjacent ancestral fossils (phylogenetic bracketing[118]). Therefore, the maximum constraint for *Mallomonas* is 228 Ma and for *Eunotia*-like raphe, 139 Ma. In addition to the constraints described above, the credibility of one putative brown algal fossil constraint, *Miaohephyton bifurcatum* (550 Ma in BACR + SSD clade) was tested. *M. bifurcatum* is a carbonaceous compression fossil from the Miaohe Member (ca. 560–550 Ma) of the Doushantuo Formation. It was previously interpreted as a possible red alga,[119] but subsequently reinterpreted as a brown alga on the basis of its dichotomously branching thalli with apical and intercalary meristems as well as specialized reproductive structures (i.e., conceptacles)[120]; these features imply that *M. bifurcatum* would be placed in the BACR + SSD clade. The brown alga interpretation has been questioned on the basis of previously published molecular clock studies that suggested a Mesozoic divergence of brown algae.[22,24,37,121] Given the possibility of morphological convergence among different algal groups, we carried out divergence time analyses with *M. bifurcatum* as a fossil calibration and checked the concordance between posterior age estimation with the prior fossil constraint (Figure S5A).

Each of the MCMC chains was run at least 2 million generations. For each condition, two independent MCMC chains were run to check the convergence. After running, individual runs were combined and convergence and mixing of parameters were checked using Tracer v1.7.2.[101] All the parameters showed > 200 effective sample sizes (ESS) values, which was a signal of good mixing. The first 200,000 traces were excluded as burn-in.

To test what clock model (uncorrelated vs. autocorrelated clock) is more proper to estimate the brown algal origin, two types of analyses were carried out. (i) We estimated the extent of autocorrelation among the different heterokont lineages with CorrTest.[33] If a lineage shows correlation of evolutionary rates among neighboring branches, autocorrelated clock model is preferred over uncorrelated model, and *vice versa*. (ii) We estimated robustness of time estimation result, comparing between the results with and without single fossil calibration point. If a time estimation with a specific clock model shows more fluctuations of the values than the other, it would be less robust in its precision.

Ancestral character estimation, transition rates, correlation and comparison analyses

Information about gamete morphology (i.e., isogamy, anisogamy and oogamy), growth site (i.e., terminal or intercalary meristems) and parthenogenetic ability (i.e., presence/absence of gamete parthenogenesis) were gleaned from the literature (Data S1C). Ancestral character estimation was conducted using the ape function in the ace library[85] in R v4.1.2.[122] 'ER (equal rates)', 'SYM (symmetric rates)' and 'ARD (all rates different)' transition models were tested and compared with likelihood-ratio tests. After that, the 'ER' model was selected and the ancestral characters on the nodes were estimated with the time tree made in the Bayesian analysis. Also, transition rates between different gamete types and correlation between gamete types and parthenogenetic ability were analyzed with BayesTraits v3.0.5.[88] Priors for both analyses were set as exponential with a mean of 10. MCMC chains were run for a million generations, and mixing and convergence were checked with Tracer v1.7.2.[101] For testing the correlated evolution between two discrete binary traits (i.e., gamete states and parthenogenetic ability), we employed a stepping stone sampler (100 stones and 1,000 iterations in each stone) that estimates the log Bayes factors of independent and dependent model of evolution.[123] Information on maximum thallus size of each species was downloaded from an online database AlgaeTraits (https://algaetraits.org/, Data S1D).[124] Whether the maximum thallus size is significantly different among distinct gamete types and sister phylogenetic lineages was compared.

Please cite this article in press as: Choi et al., Ordovician origin and subsequent diversification of the brown algae, Current Biology (2023), https://doi.org/10.1016/j.cub.2023.12.069

QUANTIFICATION AND STATISTICAL ANALYSIS

Bootstrap support for the reliability of each node was measured with ultrafast bootstrap (UFBoot). Bootstrap proportion tests such as a weighted Kishino-Hasegawa (KH), a weighted Shimodaira-Hasegawa (SH), an expected likelihood weight (ELW) and an approximately unbiased (AU) tests were performed with RELL set to 10,000 for each of the tests. In the multispecies coalescent tree, support for each node was assessed with local posterior probability. The significance of pairwise differences in thallus size between each brown algal were tested with Wilcoxon test. To estimate the effect size between estimated age distributions of different calibration scheme, we used Cohen's d.